Inverse Problems and Imaging
Volume 10, No. 2, 2016, 409–432
doi:10.3934/ipi.2016006

GHOST IMAGING IN THE RANDOM PARAXIAL REGIME

Josselin Garnier
Laboratoire de Probabilités et Modèles Aléatoires
& Laboratoire Jacques-Louis Lions
Université Paris Diderot
75205 Paris Cedex 13, France

(Communicated by Guillaume Bal)

Abstract. In this paper we analyze a wave-based imaging modality called ghost imaging that can produce an image of an object illuminated by a partially coherent source. The image of the object is obtained by correlating the intensities measured by two detectors, one that does not view the object and another one that does view the object. More exactly, a high-resolution detector measures the intensity of a wave field emitted by a partially coherent source which has not interacted with the object to be imaged. A bucket (or single-pixel) detector collects the total (spatially-integrated) intensity of the wave field emitted by the same source that has interacted with the object. The correlation of the intensity measured at the high-resolution detector with the intensity measured by the bucket detector gives an image of the object. In this paper we analyze this imaging modality when the medium through which the waves propagate is random. We discuss the relation with time reversal focusing and with correlation-based imaging using ambient noise sources. We clarify the role of the partial coherence of the source and we study how scattering affects the resolution properties of the ghost imaging function in the paraxial regime: the image resolution is all the better as the source is less coherent, and all the worse as the medium is more scattering.

1. **Introduction.** In this paper we study an imaging modality called ghost imaging introduced recently in the literature. The experimental set-up proposed in [25, 5, 18, 21] is plotted in Figure 1. The waves are emitted by a partially coherent source. A beam splitter is used to generate two wave beams from this source:
- the "reference beam", labeled ①, propagates through a homogeneous or scattering medium up to a high-resolution detector that measures the spatially resolved transmitted intensity.
- the "signal beam", labeled ②, propagates through a homogeneous or scattering medium and interacts with an object to be imaged. The total (spatially-integrated) transmitted intensity is measured by a bucket detector.

This method is called ghost imaging because the high-resolution detector does not see the object to be imaged, and nevertheless a high-resolution image of the object is obtained by cross-correlating the two measured intensity signals.

In this paper we analyze the transmission problem, in which the object is a mask modeled by a transmission function. The space coordinates are denoted by $\vec{\boldsymbol{x}} = (\boldsymbol{x}, z) \in \mathbb{R}^2 \times \mathbb{R}$. The source is located in the plane $z = 0$. The propagation distance from the source to the high-resolution detector in the reference path (labeled ① in

2010 *Mathematics Subject Classification.* Primary: 35R30, 35R60; Secondary: 78A46, 78A48.
Key words and phrases. Passive sensor imaging, ambient noise sources, scattering media, ghost imaging.

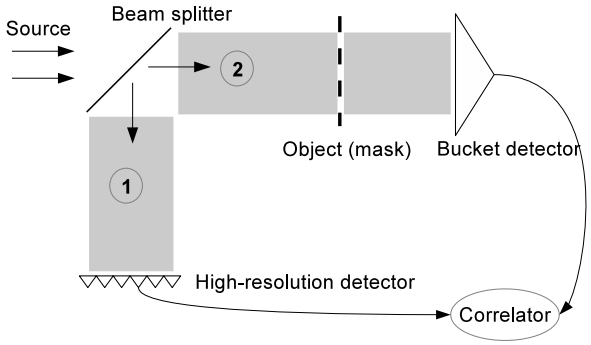

FIGURE 1. The ghost imaging setup. A partially coherent source is split into two beams by a beam splitter. The reference beam (labeled ①) does not interact with the object and its intensity is measured by a high-resolution detector. The signal beam (labeled ②) interacts with the object to be imaged and its total (spatially-integrated) intensity is measured by a bucket (single-pixel) detector.

Figure 1) is L. The propagation distance from the source to the object in the signal path (labeled ② in Figure 1) is L as well, and the propagation distance from the object to the bucket detector is L_0. In each path the scalar wave $(t,\vec{\boldsymbol{x}}) \mapsto u_j(t,\vec{\boldsymbol{x}})$, $j=1,2$, satisfies the scalar wave equation:

$$\frac{1}{c_j(\vec{\boldsymbol{x}})^2}\frac{\partial^2 u_j}{\partial t^2} - \Delta_{\vec{\boldsymbol{x}}} u_j = n(t,\boldsymbol{x})\delta(z), \tag{1}$$

where $c_j(\vec{\boldsymbol{x}})$ is the speed of propagation in the medium corresponding to the jth path and the forcing term $(t,\boldsymbol{x}) \mapsto n(t,\boldsymbol{x})$ models the source (identical for the two waves).

In the ghost experiment the source is typically a laser beam passed through a rotating glass diffuser [25, 17, 26, 21]. We model it as

$$n(t,\boldsymbol{x}) = f(t,\boldsymbol{x})e^{-i\omega_0 t} + c.c., \tag{2}$$

where $c.c.$ stands for complex conjugate, ω_0 is the carrier frequency, and $f(t,\boldsymbol{x})$ is the complex-valued, random, slowly varying envelope. It is assumed to be a complex-valued, zero-mean stationary (in time) Gaussian process with the relation and covariance functions:

$$\langle f(t,\boldsymbol{x})f(t',\boldsymbol{x}')\rangle = 0, \tag{3}$$

$$\langle f(t,\boldsymbol{x})\overline{f(t',\boldsymbol{x}')}\rangle = F(t-t')\Gamma(\boldsymbol{x},\boldsymbol{x}'), \tag{4}$$

with $F(0)=1$ and with real-valued functions F and Γ. The bandwidth (i.e., the width of the Fourier transform of F) is assumed to be much smaller than ω_0. Note that the modeling is similar to the one used for correlation-based imaging using ambient noise sources [9, 10]. We will also see in this paper that ghost imaging can be interpreted in terms of time-reversal experiments [3, 6].

In this framework the scalar wave fields u_j, $j=1,2$, can be written in the form

$$u_j(t,\vec{\boldsymbol{x}}) = v_j(t,\vec{\boldsymbol{x}})e^{-i\omega_0 t} + c.c.,$$

where v_j satisfies

$$\frac{1}{c_j(\vec{\boldsymbol{x}})^2}\frac{\partial^2}{\partial t^2}\big(v_j e^{-i\omega_0 t}\big) - \Delta_{\vec{\boldsymbol{x}}}\big(v_j e^{-i\omega_0 t}\big) = f(t,\boldsymbol{x})e^{-i\omega_0 t}\delta(z),$$

and its Fourier transform $\hat{v}_j$

$$\hat{v}_j(\omega,\vec{\boldsymbol{x}}) = \int_{-\infty}^{\infty} v_j(t,\vec{\boldsymbol{x}})\exp(i\omega t)\mathrm{d}t$$

is the solution to the Helmholtz equation:

$$\frac{(\omega_0+\omega)^2}{c_j(\vec{\boldsymbol{x}})^2}\hat{v}_j(\omega,\vec{\boldsymbol{x}}) + \Delta_{\vec{\boldsymbol{x}}}\hat{v}_j(\omega,\vec{\boldsymbol{x}}) = -\hat{f}(\omega,\boldsymbol{x})\delta(z). \tag{5}$$

The detectors measure the intensities, which means that the detectors record the square moduli of v_j, $j = 1, 2$. The goal is to image the object located along the signal path in the plane $z = L$ and that we model as a transmission function. In the experiments, the object is a mask, typically a double slit [17, 26, 21].

In Section 2, we express the correlation function of the intensities recorded by the high-resolution detector and by the bucket detector in terms of the Green's functions in the two paths, the source covariance function, and the transmission function (Proposition 1). In Section 3 we describe the statistical properties of the Green's functions in the random paraxial regime. In Section 4 we show that the correlation function takes the form (34) (Proposition 5) in the random paraxial regime (which is the regime corresponding to the experimental configurations when the medium is frozen in time). We give a heuristic interpretation of ghost imaging based on some analogy with time-reversal experiments in Section 5. In Section 6, by considering that the random medium, such as the turbulent atmosphere, is slowly and ergodically varying in time, we come to the conclusion that the correlation function is self-averaging with respect to the distribution of the random medium, and the mean correlation is our definition of the imaging function. The analysis of the imaging function carried out in Sections 7-8 shows that it is a smoothed version of the square transmission function, with a kernel that can be analyzed quantitatively. This analysis clarifies the role of the coherence of the source and the one of the scattering properties of the medium. It gives resolution formulas in terms of the propagation distance, the central wavelength and the correlation radius of the source, the correlation radius of the medium and the scattering mean free path, which are defined in terms of the two-point statistics of the random medium. The overall result is that the image resolution is all the better as the source is less coherent, and all the worse as the medium is more scatttering.

Remark 1. Ghost imaging is related to holography in that both techniques use the interaction of a signal beam that interacts with the object to be imaged and of a reference beam that does not. The goal of holography is to record and to display an image of an object, say a mask. There are two steps in holography: the recording step and the displaying step [15].

- In the recording step, a time-harmonic plane wave (or more generally a coherent light beam) is splitted into two beams by a beam splitter. One of the beams (the signal beam) interacts with the object, the other one (the reference beam) does not. The two beams interfer in a plane where a medium (a film very similar to photographic film) records the intensity of the interference

pattern. This pattern is the hologram that can be used to display an image of the object.

- In the displaying step, a beam identical to the reference beam used to record the hologram illuminates the recording medium. The recorded hologram then diffracts the beam and generates an image of the original object.

One can see that there are two main differences compared to ghost imaging:

- First, the recording medium records the intensity of the interference pattern, and the component of interest is the cross correlation of the fields corresponding to the reference beam and the signal beam. The main point of this paper is to show that it is possible to use intensity correlations instead of field correlations to do imaging.
- Second, holography requires the use of coherent light, while ghost imaging requires the use of incoherent light. This is related to the use of intensity correlations as explained in this paper.

2. **The empirical and statistical correlations.** The quantity that is measured by the high-resolution detector is the spatially-resolved intensity in the plane $z = L$ of the reference path ①:

$$I_1(t, \boldsymbol{x}_1) = \big|v_1\big(t, (\boldsymbol{x}_1, L)\big)\big|^2. \tag{6}$$

The quantity that is measured by the bucket detector is the spatially-integrated intensity in the plane $z = L + L_0$ of the signal path ②:

$$I_2(t) = \int_{\mathbb{R}^2} \big|v_2\big(t, (\boldsymbol{x}_2, L + L_0)\big)\big|^2 \mathrm{d}\boldsymbol{x}_2. \tag{7}$$

These two quantities are correlated and this gives the empirical intensity correlation function:

$$\begin{aligned} \mathcal{C}_T(\boldsymbol{x}_1) &= \frac{1}{T}\int_0^T I_1(t, \boldsymbol{x}_1) I_2(t) \mathrm{d}t \\ &\quad - \Big[\frac{1}{T}\int_0^T I_1(t, \boldsymbol{x}_1)\mathrm{d}t\Big]\Big[\frac{1}{T}\int_0^T I_2(t)\mathrm{d}t\Big]. \end{aligned} \tag{8}$$

From (5) we can express the reference field $\hat{v}_1$ at point $\vec{\boldsymbol{x}}_1 = (\boldsymbol{x}_1, L)$ in the plane $z = L$ of the high-resolution detector as

$$\hat{v}_1(\omega, \vec{\boldsymbol{x}}_1) = \int_{\mathbb{R}^2} \hat{\mathcal{G}}_1\big(\omega_0 + \omega, \vec{\boldsymbol{x}}_1, (\boldsymbol{x}_s, 0)\big)\hat{f}(\omega, \boldsymbol{x}_s)\mathrm{d}\boldsymbol{x}_s,$$

in terms of the full Green's function $\hat{\mathcal{G}}_1$ in the reference path and the Fourier transform $\hat{f}$ of the source. Similarly we express the signal field $\hat{v}_2$ at point $\vec{\boldsymbol{x}}_2 = (\boldsymbol{x}_2, L + L_0)$ in the plane $z = L + L_0$ of the bucket detector as

$$\hat{v}_2(\omega, \vec{\boldsymbol{x}}_2) = \int_{\mathbb{R}^2} \hat{\mathcal{G}}_2\big(\omega_0 + \omega, \vec{\boldsymbol{x}}_2, (\boldsymbol{x}_s, 0)\big)\hat{f}(\omega, \boldsymbol{x}_s)\mathrm{d}\boldsymbol{x}_s,$$

in terms of the full Green's function $\hat{\mathcal{G}}_2$ in the signal path. In this section we assume that the media in the reference and signal paths are frozen (i.e. they are time-independent).

Proposition 1. *We have convergence in probability of the empirical correlation to the statistical correlation:*

$$\mathcal{C}_T(\boldsymbol{x}_1) \overset{T\to\infty}{\longrightarrow} \mathcal{C}(\boldsymbol{x}_1),$$

with the statistical correlation given by

$$\begin{aligned}\mathcal{C}(\boldsymbol{x}_1) &= \frac{1}{4\pi^2}\int_{-\infty}^{\infty}\mathrm{d}\omega\int_{-\infty}^{\infty}\mathrm{d}\omega'\int_{\mathbb{R}^2}\mathrm{d}\boldsymbol{y}_1\int_{\mathbb{R}^2}\mathrm{d}\boldsymbol{y}_1'\int_{\mathbb{R}^2}\mathrm{d}\boldsymbol{y}_2\int_{\mathbb{R}^2}\mathrm{d}\boldsymbol{y}_2'\int_{\mathbb{R}^2}\mathrm{d}\boldsymbol{x}_2\\ &\times\hat{\mathcal{G}}_1\big(\omega_0+\omega,(\boldsymbol{x}_1,L),(\boldsymbol{y}_1,0)\big)\overline{\hat{\mathcal{G}}_1\big(\omega_0+\omega',(\boldsymbol{x}_1,L),(\boldsymbol{y}_1',0)\big)}\\ &\times\overline{\hat{\mathcal{G}}_2\big(\omega_0+\omega,(\boldsymbol{x}_2,L+L_0),(\boldsymbol{y}_2,0)\big)}\hat{\mathcal{G}}_2\big(\omega_0+\omega',(\boldsymbol{x}_2,L+L_0),(\boldsymbol{y}_2',0)\big)\\ &\times\Gamma(\boldsymbol{y}_1,\boldsymbol{y}_2)\Gamma(\boldsymbol{y}_1',\boldsymbol{y}_2')\hat{F}(\omega)\hat{F}(\omega'). \qquad (9)\end{aligned}$$

Proof. The convergence in probability can be proved in the same way as in [9, 11] by showing that the variance of $\mathcal{C}_T$ is proportional to $1/T$ and using Chebyshef's inequality. The statistical cross correlation is given by

$$\begin{aligned}\mathcal{C}(\boldsymbol{x}_1) &= \int_{\mathbb{R}^2}\langle\big|v_1\big(0,(\boldsymbol{x}_1,L)\big)\big|^2\big|v_2\big(0,(\boldsymbol{x}_2,L+L_0)\big)\big|^2\rangle\mathrm{d}\boldsymbol{x}_2\\ &\quad-\langle\big|v_1\big(0,(\boldsymbol{x}_1,L)\big)\big|^2\rangle\int_{\mathbb{R}^2}\langle\big|v_2\big(0,(\boldsymbol{x}_2,L+L_0)\big)\big|^2\rangle\mathrm{d}\boldsymbol{x}_2.\end{aligned}$$

In the Fourier domain, the source term is a complex-valued Gaussian process with the relation and covariance functions

$$\langle\hat{f}(\omega,\boldsymbol{x})\hat{f}(\omega',\boldsymbol{x}')\rangle = 0, \qquad (10)$$

$$\langle\hat{f}(\omega,\boldsymbol{x})\overline{\hat{f}(\omega',\boldsymbol{x}')}\rangle = 2\pi\delta(\omega-\omega')\hat{F}(\omega)\Gamma(\boldsymbol{x},\boldsymbol{x}'). \qquad (11)$$

By using the Fourier form, we get:

$$\begin{aligned}\mathcal{C}(\boldsymbol{x}_1) &= \frac{1}{(2\pi)^4}\int_{\mathbb{R}^2}\mathrm{d}\boldsymbol{y}_1\int_{\mathbb{R}^2}\mathrm{d}\boldsymbol{y}_1'\int_{\mathbb{R}^2}\mathrm{d}\boldsymbol{y}_2\int_{\mathbb{R}^2}\mathrm{d}\boldsymbol{y}_2'\int_{\mathbb{R}^2}\mathrm{d}\boldsymbol{x}_2\\ &\times\int_{-\infty}^{\infty}\mathrm{d}\omega_1\int_{-\infty}^{\infty}\mathrm{d}\omega_1'\int_{-\infty}^{\infty}\mathrm{d}\omega_2\int_{-\infty}^{\infty}\mathrm{d}\omega_2'\\ &\times\hat{\mathcal{G}}_1\big(\omega_0+\omega_1,(\boldsymbol{x}_1,L),(\boldsymbol{y}_1,0)\big)\overline{\hat{\mathcal{G}}_1\big(\omega_0+\omega_1',(\boldsymbol{x}_1,L),(\boldsymbol{y}_1',0)\big)}\\ &\times\overline{\hat{\mathcal{G}}_2\big(\omega_0+\omega_2,(\boldsymbol{x}_2,L+L_0),(\boldsymbol{y}_2,0)\big)}\hat{\mathcal{G}}_2\big(\omega_0+\omega_2',(\boldsymbol{x}_2,L+L_0),(\boldsymbol{y}_2',0)\big)\\ &\times\Big[\langle\hat{f}(\omega_1,\boldsymbol{y}_1)\overline{\hat{f}(\omega_1',\boldsymbol{y}_1')\hat{f}(\omega_2,\boldsymbol{y}_2)}\hat{f}(\omega_2',\boldsymbol{y}_2')\rangle\\ &\quad-\langle\hat{f}(\omega_1,\boldsymbol{y}_1)\overline{\hat{f}(\omega_1',\boldsymbol{y}_1')}\rangle\langle\overline{\hat{f}(\omega_2,\boldsymbol{y}_2)}\hat{f}(\omega_2',\boldsymbol{y}_2')\rangle\Big].\end{aligned}$$

By the Gaussian property of the noise source, we have

$$\begin{aligned}&\langle\hat{f}(\omega_1,\boldsymbol{y}_1)\overline{\hat{f}(\omega_1',\boldsymbol{y}_1')\hat{f}(\omega_2,\boldsymbol{y}_2)}\hat{f}(\omega_2',\boldsymbol{y}_2')\rangle\\ &\quad-\langle\hat{f}(\omega_1,\boldsymbol{y}_1)\overline{\hat{f}(\omega_1',\boldsymbol{y}_1')}\rangle\langle\overline{\hat{f}(\omega_2,\boldsymbol{y}_2)}\hat{f}(\omega_2',\boldsymbol{y}_2')\rangle\\ &=\langle\hat{f}(\omega_1,\boldsymbol{y}_1)\overline{\hat{f}(\omega_2,\boldsymbol{y}_2)}\rangle\langle\overline{\hat{f}(\omega_1',\boldsymbol{y}_1')}\hat{f}(\omega_2',\boldsymbol{y}_2')\rangle\\ &\quad+\langle\hat{f}(\omega_1,\boldsymbol{y}_1)\hat{f}(\omega_2',\boldsymbol{y}_2')\rangle\langle\overline{\hat{f}(\omega_1',\boldsymbol{y}_1')\hat{f}(\omega_2,\boldsymbol{y}_2)}\rangle\\ &=(2\pi)^2\Gamma(\boldsymbol{y}_1,\boldsymbol{y}_2)\Gamma(\boldsymbol{y}_1',\boldsymbol{y}_2')\hat{F}(\omega_1)\hat{F}(\omega_1')\delta(\omega_1-\omega_2)\delta(\omega_1'-\omega_2'),\end{aligned}$$

which gives the desired result. □

As shown by the expression (9) in Proposition 1, the products of two Green's functions (one of them being complex conjugated) play a central role in the understanding of ghost imaging and we will describe their statistical properties in the random paraxial regime in the next section.

3. Overview of the random paraxial model.

3.1. **The random paraxial regime.** In this section we introduce and analyze a scaling regime in which scattering is isotropic and weak, which allows us to use the random paraxial wave model to describe the wave propagation in the scattering region. In this regime, backscattering is negligible but there is significant lateral scattering as the wave advances over long propagation distances. Even though they are weak, these effects accumulate and can be a limiting factor in imaging and communications if not mitigated in some way. Wave propagation in random media in the paraxial regime has been used extensively in underwater sound propagation as well as in the microwave and optical contexts in the atmosphere [24, 22]. We formulate the regime of paraxial wave propagation in random media with a scaling of parameters that allows detailed and effective mathematical analysis [12]. It is described as follows.

1) We assume that the correlation length l_c of the medium is much smaller than the typical propagation distance L. We denote by ε^2 the ratio between the correlation length and the typical propagation distance:

$$\frac{l_c}{L} \sim \varepsilon^2.$$

2) We assume that the transverse width of the source R_0 and the correlation length of the medium l_c are of the same order. This means that the ratio R_0/L is of order ε^2. This scaling is motivated by the fact that, in this regime, there is a non-trivial interaction between the fluctuations of the medium and the wave.

3) We assume that the typical wavelength λ is much smaller than the propagation distance L, more precisely, we assume that the ratio λ/L is of order ε^4. This high-frequency scaling is motivated by the following considerations. The Rayleigh length for a beam with initial width R_0 and central wavelength λ is of the order of R_0^2/λ when there is no random fluctuation. The Rayleigh length is the distance from beam waist where the beam area is doubled by diffraction [4]. In order to get a Rayleigh length of the order of the propagation distance L, the ratio λ/L must be of order ε^4 since $R_0/L \sim \varepsilon^2$:

$$\frac{\lambda}{L} \sim \varepsilon^4.$$

4) We assume that the typical amplitude of the random fluctuations of the medium is small. More precisely, we assume that the relative amplitude of the fluctuations is of order ε^3. This scaling has been chosen so as to obtain an effective regime of order one when ε goes to zero. That is, if the magnitude of the fluctuations is smaller than ε^3, then the wave would propagate as if the medium was homogeneous, while if the order of magnitude is larger, then the wave would not be able to penetrate the random medium. The scaling that we consider here corresponds to the physically most interesting situation where random effects play a role.

3.2. **The random paraxial wave equation.** We consider the time-harmonic form of the scalar wave equation:

$$\Delta_{\vec{\boldsymbol{x}}}\hat{u} + \frac{\omega^2}{c^2(\vec{\boldsymbol{x}})}\hat{u} = 0,$$

with the speed of propagation in the medium of the form

$$\frac{1}{c^2(\vec{\boldsymbol{x}})} = \frac{1}{c_0^2}\big(1+\mu(\boldsymbol{x},z)\big), \tag{12}$$

where μ is a zero-mean, stationary, three-dimensional random process with mixing properties in the z-direction. Therefore the time-harmonic wave field is solution to the random Helmholtz equation:

$$(\partial_z^2+\Delta_{\boldsymbol{x}})\hat{u} + \frac{\omega^2}{c_0^2}\big(1+\mu(\boldsymbol{x},z)\big)\hat{u} = 0, \tag{13}$$

where $\Delta_{\boldsymbol{x}}$ is the transverse Laplacian (i.e. the Laplacian with respect to $\boldsymbol{x}$). In the high-frequency regime described in the previous subsection,

$$\omega \to \frac{\omega}{\varepsilon^4}, \qquad \mu(\boldsymbol{x},z) \to \varepsilon^3\mu\big(\frac{\boldsymbol{x}}{\varepsilon^2},\frac{z}{\varepsilon^2}\big), \tag{14}$$

the rescaled function $\hat{\phi}^\varepsilon$ defined by

$$\hat{u}^\varepsilon(\omega,\boldsymbol{x},z) = \exp\Big(i\frac{\omega}{\varepsilon^4}\frac{z}{c_0}\Big)\hat{\phi}^\varepsilon\Big(\omega,\frac{\boldsymbol{x}}{\varepsilon^2},z\Big) \tag{15}$$

satisfies

$$\varepsilon^4\partial_z^2\hat{\phi}^\varepsilon + \left(2i\frac{\omega}{c_0}\partial_z\hat{\phi}^\varepsilon + \Delta_{\boldsymbol{x}}\hat{\phi}^\varepsilon + \frac{\omega^2}{\varepsilon c_0^2}\mu\big(\boldsymbol{x},\frac{z}{\varepsilon^2}\big)\hat{\phi}^\varepsilon\right) = 0. \tag{16}$$

The ansatz (15) corresponds to a plane wave propagating along the z-axis with a slowly varying transverse envelope. In the regime $\varepsilon \ll 1$, it has been shown in [12] that the forward-scattering approximation in the negative z-direction and the white-noise approximation are valid, which means that the second-order derivative in z in (16) can be neglected and the random potential $\frac{1}{\varepsilon}\mu\big(\boldsymbol{x},\frac{z}{\varepsilon^2}\big)$ can be replaced by a white noise. The mathematical statement is that the function $\hat{\phi}^\varepsilon(\omega,\boldsymbol{x},z)$ weakly converges to the solution $\hat{\phi}(\omega,\boldsymbol{x},z)$ of the Itô-Schrödinger equation

$$2i\frac{\omega}{c_0}\mathrm{d}_z\hat{\phi}(\omega,\boldsymbol{x},z) + \Delta_{\boldsymbol{x}}\hat{\phi}(\omega,\boldsymbol{x},z)\mathrm{d}z + \frac{\omega^2}{c_0^2}\hat{\phi}(\omega,\boldsymbol{x},z)\circ\mathrm{d}B(\boldsymbol{x},z) = 0, \tag{17}$$

where $B(\boldsymbol{x},z)$ is a Brownian field, that is a Gaussian process with mean zero and covariance function

$$\mathbb{E}\big[B(\boldsymbol{x},z)B(\boldsymbol{x}',z')\big] = \gamma_0(\boldsymbol{x}-\boldsymbol{x}')\big(z\wedge z'\big), \tag{18}$$

with

$$\gamma_0(\boldsymbol{x}) = \int_{-\infty}^{\infty}\mathbb{E}[\mu(\mathbf{0},0)\mu(\boldsymbol{x},z)]\mathrm{d}z. \tag{19}$$

Here the $\circ$ stands for the Stratonovich stochastic integral [12]. In Itô's form this equation reads as:

$$\begin{aligned}\mathrm{d}_z\hat{\phi}(\omega,\boldsymbol{x},z) \quad &= \quad \frac{ic_0}{2\omega}\Delta_{\boldsymbol{x}}\hat{\phi}(\omega,\boldsymbol{x},z)\mathrm{d}z + \frac{i\omega}{2c_0}\hat{\phi}(\omega,\boldsymbol{x},z)\mathrm{d}B(\boldsymbol{x},z)\\ &\quad -\frac{\omega^2\gamma_0(\mathbf{0})}{8c_0^2}\hat{\phi}(\omega,\boldsymbol{x},z)\mathrm{d}z.\end{aligned} \tag{20}$$

3.3. **The moments of the fundamental solution.** We introduce the fundamental solution $\hat{g}\big(\omega,(\boldsymbol{x},z),(\boldsymbol{x}_0,z_0)\big)$, which is defined as the solution of the equation in $(\boldsymbol{x},z)$ (for $z>z_0$):

$$2i\frac{\omega}{c_0}\mathrm{d}_z\hat{g}+\Delta_{\boldsymbol{x}}\hat{g}\mathrm{d}z+\frac{\omega^2}{c_0^2}\hat{g}\circ\mathrm{d}B(\boldsymbol{x},z)=0, \tag{21}$$

starting from $\hat{g}\big(\omega,(\boldsymbol{x},z=z_0),(\boldsymbol{x}_0,z_0)\big)=\delta(\boldsymbol{x}-\boldsymbol{x}_0)$. In a homogeneous medium ($B\equiv 0$) the fundamental solution is (for $z>z_0$)

$$\hat{g}_0\big(\omega,(\boldsymbol{x},z),(\boldsymbol{x}_0,z_0)\big)=\frac{\omega}{2i\pi c_0(z-z_0)}\exp\Big(i\frac{\omega|\boldsymbol{x}-\boldsymbol{x}_0|^2}{2c_0(z-z_0)}\Big). \tag{22}$$

In a random medium, the first two moments of the random fundamental solution have the following expressions.

Proposition 2. *The first order-moment of the random fundamental solution exhibits frequency-dependent damping (for $z>z_0$):*

$$\mathbb{E}\big[\hat{g}\big(\omega,(\boldsymbol{x},z),(\boldsymbol{x}_0,z_0)\big)\big]=\hat{g}_0\big(\omega,(\boldsymbol{x},z),(\boldsymbol{x}_0,z_0)\big)\exp\Big(-\frac{\gamma_0(\boldsymbol{0})\omega^2(z-z_0)}{8c_0^2}\Big), \tag{23}$$

where γ_0 is given by (19).

The second order-moment of the random fundamental solution exhibits spatial decorrelation:

$$\begin{aligned}&\mathbb{E}\big[\hat{g}\big(\omega,(\boldsymbol{x},z),(\boldsymbol{x}_0,z_0)\big)\overline{\hat{g}\big(\omega,(\boldsymbol{x}',z),(\boldsymbol{x}_0,z_0)\big)}\big]\\ &=\hat{g}_0\big(\omega,(\boldsymbol{x},z),(\boldsymbol{x}_0,z_0)\big)\overline{\hat{g}_0\big(\omega,(\boldsymbol{x}',z),(\boldsymbol{x}_0,z_0)\big)}\exp\Big(-\frac{\gamma_2(\boldsymbol{x}-\boldsymbol{x}')\omega^2(z-z_0)}{4c_0^2}\Big),\end{aligned} \tag{24}$$

where

$$\gamma_2(\boldsymbol{x})=\int_0^1\gamma_0(\boldsymbol{0})-\gamma_0(\boldsymbol{x}s)\mathrm{d}s. \tag{25}$$

These are classical results [16, Chapter 20] once the the random paraxial equation has been proved to be correct, as is the case here. For consistency we give the proof in Appendix B. The result (23) on the first-order moment shows that any coherent wave imaging method cannot give good images if the propagation distance is larger than the scattering mean free path:

$$l_{\mathrm{sca}}=\frac{8c_0^2}{\gamma_0(\boldsymbol{0})\omega^2}, \tag{26}$$

because the coherent wave components will then be exponentially damped. This is the situation we have in mind, and this is the situation in which correlation-based imaging turns out to be efficient.

In the next proposition we address the strongly scattering regime, that is, the regime when the propagation distance is larger than the scattering mean free path.

Proposition 3. *Let us assume that the covariance function γ_0 can be expanded as*

$$\gamma_0(\boldsymbol{x})=\gamma_0(\boldsymbol{0})\Big[1-\frac{|\boldsymbol{x}|^2}{l_{\mathrm{cor}}^2}+o\Big(\frac{|\boldsymbol{x}|^2}{l_{\mathrm{cor}}^2}\Big)\Big],\qquad \frac{|\boldsymbol{x}|}{l_{\mathrm{cor}}}\ll 1, \tag{27}$$

where $l_{\rm cor}$ is the correlation radius of the medium. In the strongly scattering regime $|z-z_0| \gg l_{\rm sca}$, the first order-moment of the random fundamental solution is vanishing and the second order-moment is given by:

$$\begin{aligned}&\mathbb{E}\big[\hat{g}\big(\omega,(\boldsymbol{x},z),(\boldsymbol{x}_0,z_0)\big)\overline{\hat{g}\big(\omega,(\boldsymbol{x}',z),(\boldsymbol{x}_0,z_0)\big)}\big]\\ &=\hat{g}_0\big(\omega,(\boldsymbol{x},z),(\boldsymbol{x}_0,z_0)\big)\overline{\hat{g}_0\big(\omega,(\boldsymbol{x}',z),(\boldsymbol{x}_0,z_0)\big)}\exp\Big(-\frac{|\boldsymbol{x}-\boldsymbol{x}'|^2}{2X_c^2}\Big),\end{aligned} \tag{28}$$

where

$$X_c=\frac{\sqrt{3}}{2}\frac{l_{\rm cor}\sqrt{l_{\rm sca}}}{\sqrt{z-z_0}}. \tag{29}$$

If, for instance, the covariance function of the medium fluctuations has the form

$$\mathbb{E}\big[\mu(\vec{\boldsymbol{x}})\mu(\vec{\boldsymbol{x}}')\big]=\sigma^2\exp\Big(-\frac{\pi|\vec{\boldsymbol{x}}-\vec{\boldsymbol{x}}'|^2}{l_{\rm cor}^2}\Big),$$

then the scattering mean free path and the decoherence length for the Green's function are

$$l_{\rm sca}=\frac{8c_0^2}{\sigma^2 l_{\rm cor}\omega^2},\qquad X_c=\frac{\sqrt{6}c_0\sqrt{l_{\rm cor}}}{\sigma\sqrt{\pi}\omega\sqrt{z-z_0}}.$$

The following proposition describes the spreading of a Gaussian beam and it is proved in Appendix C.

Proposition 4. *Let us consider an initial condition in the plane $z=0$ in the form of a Gaussian beam with initial radius $r_{\rm ic}$:*

$$\hat{\phi}(\omega,\boldsymbol{x},z=0)=\exp\Big(-\frac{|\boldsymbol{x}|^2}{2r_{\rm ic}^2}\Big). \tag{30}$$

In the strongly scattering regime $z\gg l_{\rm sca}$, the mean intensity profile is a Gaussian beam with radius $R(\omega,z)$:

$$\mathbb{E}[|\hat{\phi}(\omega,\boldsymbol{x},z)|^2]=\frac{r_{\rm ic}^2}{R^2(\omega,z)}\exp\Big(-\frac{|\boldsymbol{x}|^2}{R^2(\omega,z)}\Big),$$

with

$$R^2(\omega,z)=r_{\rm ic}^2+\frac{c_0^2z^2}{\omega^2r_{\rm ic}^2}+\frac{8c_0^2z^3}{3\omega^2l_{\rm cor}^2l_{\rm sca}}. \tag{31}$$

Note that $r_{\rm ic}^2+\frac{c_0^2z^2}{r_{\rm ic}^2\omega^2}$ is the formula for the square radius of a Gaussian beam that undergoes classical diffraction in a homogeneous medium with speed of propagation c_0. The last term $\frac{8c_0^2z^3}{3\omega^2l_{\rm cor}^2l_{\rm sca}}$ is induced by scattering in the random medium and it shows that beam spreading is enhanced by scattering.

4. **Ghost imaging in the paraxial regime.** In this paper we study ghost imaging in the paraxial regime, that is the regime in which the propagation distance is much larger than the correlation length of the medium, which is itself much larger than the typical wavelength, as in the previous section. Accordingly, we introduce a dimensionless parameter ε that quantifies these scaling ratios and assume that the typical wavelength is of order ε^4, the correlation length of the medium and the radius of the beam is of order ε^2, and the object itself has a size of order ε^2 comparable to the size of the propagating beam. Moreover, in the optical ghost imaging experiments, the partially coherent wave is generated by passing a monochromatic laser beam through a rotating diffuser [17]. The induced time fluctuations have

a decoherence time much longer than the oscillation frequency of the monochromatic laser beam, so we shall assume that the decoherence time is of order ε^p, with $p \in (0,4)$.

To summarize, we consider that the carrier frequency is ω_0/ε^4, the source term is of the form

$$f^\varepsilon(t,\boldsymbol{x}) = f\Big(\frac{t}{\varepsilon^p}, \frac{\boldsymbol{x}}{\varepsilon^2}\Big), \tag{32}$$

and the (real-valued) transmission function that models the object is

$$\mathcal{T}^\varepsilon(\boldsymbol{y}) = \mathcal{T}\Big(\frac{\boldsymbol{y}}{\varepsilon^2}\Big). \tag{33}$$

As shown in Appendix A, the slowly varying envelope of the reference field in the plane of the high-resolution detector $z = L$ at the point $\vec{\boldsymbol{x}}_1^\varepsilon = (\varepsilon^2\boldsymbol{x}_1, L)$ is

$$\begin{aligned}\hat{v}_1^\varepsilon\Big(\frac{\omega}{\varepsilon^p}, \vec{\boldsymbol{x}}_1^\varepsilon\Big) \quad \stackrel{\varepsilon\to 0}{\longrightarrow} \quad & \frac{ic_0\varepsilon^{4+p}}{2\omega_0}\exp\Big(i\big(\frac{\omega_0}{\varepsilon^4}+\frac{\omega}{\varepsilon^p}\big)\frac{L}{c_0}\Big)\\ & \times\int_{\mathbb{R}^2}\hat{g}_1\big(\omega_0,(\boldsymbol{x}_1,L),(\boldsymbol{y}_1,0)\big)\hat{f}(\omega,\boldsymbol{y}_1)\mathrm{d}\boldsymbol{y}_1,\end{aligned}$$

where $\hat{g}_1$ is the fundamental solution of the Itô-Schrödinger equation (21) in the reference path. This expression means that the wave propagates from the source plane $z = 0$ to the high-resolution detector plane $z = L$ in the white-noise paraxial regime.

As shown in Appendix A, the slowly varying envelope of the signal field in the plane of the bucket detector $z = L + L_0$ at the point $\vec{\boldsymbol{x}}_2^\varepsilon = (\varepsilon^2\boldsymbol{x}_2, L + L_0)$ is

$$\begin{aligned}\hat{v}_2^\varepsilon\Big(\frac{\omega}{\varepsilon^p}, \vec{\boldsymbol{x}}_2^\varepsilon\Big) \quad \stackrel{\varepsilon\to 0}{\longrightarrow} \quad & \frac{ic_0\varepsilon^{4+p}}{2\omega_0}\exp\Big(i\big(\frac{\omega_0}{\varepsilon^4}+\frac{\omega}{\varepsilon^p}\big)\frac{L+L_0}{c_0}\Big)\\ & \times\int_{\mathbb{R}^2}\int_{\mathbb{R}^2}\hat{g}_2\big(\omega_0,(\boldsymbol{x}_2,L+L_0),(\boldsymbol{y},L)\big)\\ & \times\mathcal{T}(\boldsymbol{y})\hat{g}_2\big(\omega_0,(\boldsymbol{y},L),(\boldsymbol{y}_2,0)\big)\hat{f}(\omega,\boldsymbol{y}_2)\mathrm{d}\boldsymbol{y}_2\mathrm{d}\boldsymbol{y},\end{aligned}$$

where $\hat{g}_2$ is the fundamental solution of the Itô-Schrödinger equation in the signal path. This expression means that the wave propagates from the source plane $z = 0$ to the object plane $z = L$ in the white-noise paraxial regime, it goes through a mask as described by the transmission function $\mathcal{T}$, and it propagates from the object plane $z = L$ to the bucket detector plane $z = L + L_0$ in the white-noise paraxial regime.

Based on these expressions, and using Proposition 1 and the fact that $\int \hat{F}(\omega)\mathrm{d}\omega = 2\pi F(0) = 2\pi$, we get the following result.

Proposition 5. *In the white-noise paraxial regime $\varepsilon \to 0$, the statistical correlation is given by*

$$\varepsilon^{-20}\mathcal{C}^\varepsilon(\varepsilon^2\boldsymbol{x}_1) \stackrel{\varepsilon\to 0}{\longrightarrow} \mathcal{C}_p(\boldsymbol{x}_1),$$

with

$$\begin{aligned}\mathcal{C}_p(\boldsymbol{x}_1) = \frac{c_0^4}{16\omega_0^4}\int_{\mathbb{R}^2}\mathrm{d}\boldsymbol{y}_1\int_{\mathbb{R}^2}\mathrm{d}\boldsymbol{y}_1'\int_{\mathbb{R}^2}\mathrm{d}\boldsymbol{y}_2\int_{\mathbb{R}^2}\mathrm{d}\boldsymbol{y}_2'\int_{\mathbb{R}^2}\mathrm{d}\boldsymbol{y}_3\int_{\mathbb{R}^2}\mathrm{d}\boldsymbol{y}_3'\\ \times\int_{\mathbb{R}^2}\mathrm{d}\boldsymbol{x}_2\hat{g}_1\big(\omega_0,(\boldsymbol{x}_1,L),(\boldsymbol{y}_1,0)\big)\overline{\hat{g}_1\big(\omega_0,(\boldsymbol{x}_1,L),(\boldsymbol{y}_1',0)\big)}\\ \times\overline{\hat{g}_2\big(\omega_0,(\boldsymbol{x}_2,L+L_0),(\boldsymbol{y}_3',L)\big)}\mathcal{T}(\boldsymbol{y}_3')\overline{\hat{g}_2\big(\omega_0,(\boldsymbol{y}_3',L),(\boldsymbol{y}_2,0)\big)}\\ \times\hat{g}_2\big(\omega_0,(\boldsymbol{x}_2,L+L_0),(\boldsymbol{y}_3,L)\big)\mathcal{T}(\boldsymbol{y}_3)\hat{g}_2\big(\omega_0,(\boldsymbol{y}_3,L),(\boldsymbol{y}_2',0)\big)\\ \times\Gamma(\boldsymbol{y}_1,\boldsymbol{y}_2)\Gamma(\boldsymbol{y}_1',\boldsymbol{y}_2'),\end{aligned}\tag{34}$$

where $\hat{g}_1$, resp. $\hat{g}_2$, is the fundamental solution of the Itô-Schrödinger equation (21) in the reference path, resp. the signal path.

5. **Time-reversal heuristic interpretation.** We can now explain heuristically why we can expect the statistical correlation to give a good image of the transmission function $\mathcal{T}$. This explanation is based on a time-reversal interpretation of the statistical correlation. Let us remind the reader about time reversal for waves. A time-reversal experiment is based on the use of a special device called time-reversal mirror, which is a collection of transducers that can be used as sources and receivers. In the first step of a time-reversal experiment, the time-reversal mirror is used as an array of receivers that record the signal emitted by a source. In the second step, the time-reversal mirror is used as an array of sources that reemit the time-reversed recorded signals (or equivalently the complex conjugates of the Fourier transforms). The main effect is the refocusing of the time-reversed waves on the original source location [6].

Let us consider the statistical correlation (34) when the source is spatially incoherent so that $\Gamma(\boldsymbol{x},\boldsymbol{x}') = K(\boldsymbol{x})\delta(\boldsymbol{x}-\boldsymbol{x}')$. Then

$$\begin{aligned}\mathcal{C}_p(\boldsymbol{x}_1) = \frac{c_0^4}{16\omega_0^4}\int_{\mathbb{R}^2}\mathrm{d}\boldsymbol{y}_3\int_{\mathbb{R}^2}\mathrm{d}\boldsymbol{y}_3'\mathcal{T}(\boldsymbol{y}_3)\mathcal{T}(\boldsymbol{y}_3')\\ \times\int_{\mathbb{R}^2}\mathrm{d}\boldsymbol{y}_1\hat{g}_1\big(\omega_0,(\boldsymbol{x}_1,L),(\boldsymbol{y}_1,0)\big)\overline{\hat{g}_2\big(\omega_0,(\boldsymbol{y}_3',L),(\boldsymbol{y}_1,0)\big)}K(\boldsymbol{y}_1)\\ \times\int_{\mathbb{R}^2}\mathrm{d}\boldsymbol{y}_1'\overline{\hat{g}_1\big(\omega_0,(\boldsymbol{x}_1,L),(\boldsymbol{y}_1',0)\big)}\hat{g}_2\big(\omega_0,(\boldsymbol{y}_3,L),(\boldsymbol{y}_1',0)\big)K(\boldsymbol{y}_1')\\ \times\int_{\mathbb{R}^2}\mathrm{d}\boldsymbol{x}_2\overline{\hat{g}_2\big(\omega_0,(\boldsymbol{x}_2,L+L_0),(\boldsymbol{y}_3',L)\big)}\hat{g}_2\big(\omega_0,(\boldsymbol{x}_2,L+L_0),(\boldsymbol{y}_3,L)\big).\end{aligned}$$

The integral in $\mathrm{d}\boldsymbol{y}_1$ gives the result of a time-reversal experiment using a point source at $(\boldsymbol{y}_3',L)$, a time-reversal mirror in the plane $z=0$ with the transverse support described by the function K, and an observation point at $(\boldsymbol{x}_1,L)$. We can anticipate from the refocusing properties of time reversal that it is concentrated at $\boldsymbol{x}_1=\boldsymbol{y}_3'$. Similarly, we can anticipate that the integral in $\mathrm{d}\boldsymbol{y}_1'$ is concentrated at $\boldsymbol{x}_1=\boldsymbol{y}_3$ and the last integral in $\mathrm{d}\boldsymbol{x}_2$ is concentrated at $\boldsymbol{y}_3'=\boldsymbol{y}_3$. As a result, when one integrates against the function $\mathcal{T}(\boldsymbol{y}_3)\mathcal{T}(\boldsymbol{y}_3')$ in $\boldsymbol{y}_3'$ and $\boldsymbol{y}_3$, then one can anticipate that the result should be proportional to $\mathcal{T}(\boldsymbol{x}_1)^2$, which means that the statistical correlation should be an image of the square transmission function $\mathcal{T}$.

This heuristic explanation is in fact very close to reality when the medium is homogeneous, because then $\hat{g}_1=\hat{g}_2=\hat{g}_0$, where $\hat{g}_0$ is the homogeneous fundamental solution (22). However, when the medium is random, the reference and signal waves travel through two different realizations of the random medium, so that $\hat{g}_1$ and

$\hat{g}_2$ may have the same statistics but they are independent. In the time-reversal interpretation, this means that the wave backpropagates in a different realization of the random medium. We know that time-reversal refocusing is sensitive to any change in the medium [1, 2], so we can anticipate that random scattering is not good for ghost imaging.

The next sections will confirm and quantify these heuristic explanations.

6. Averaging with respect to the random medium.

We consider the ghost imaging function defined as the mean correlation

$$\mathcal{I}_{\rm gi}(\boldsymbol{x}_1) = \mathbb{E}[\mathcal{C}_p(\boldsymbol{x}_1)], \tag{35}$$

where the expectation is taken with respect to the random media in the reference path (labeled ①) and signal path (labeled ②). It is indeed justified to take such an expectation in the experimental conditions considered in ghost imaging, in which the random medium is the turbulent atmosphere. The turbulent atmosphere is slowly and ergodically varying in time (with a coherence time of the order of a few milliseconds, as described in [16, Vol. 2], [21], or [23]). If the integration time T is longer than this coherence time, then the empirical correlation is self-averaging with respect to the distribution of the random medium.

Proposition 6. *The ghost imaging function is related to the square transmission function through the relation*

$$\mathcal{I}_{\rm gi}(\boldsymbol{x}_1) = \int_{\mathbb{R}^2} \mathrm{d}\boldsymbol{y}_3 H(\boldsymbol{x}_1,\boldsymbol{y}_3)\mathcal{T}(\boldsymbol{y}_3)^2, \tag{36}$$

with the kernel

$$\begin{aligned} H(\boldsymbol{x}_1,\boldsymbol{y}_3) \;=\; & \frac{c_0^4}{16\omega_0^4}\int_{\mathbb{R}^2}\mathrm{d}\boldsymbol{y}_1\int_{\mathbb{R}^2}\mathrm{d}\boldsymbol{y}_1'\int_{\mathbb{R}^2}\mathrm{d}\boldsymbol{y}_2\int_{\mathbb{R}^2}\mathrm{d}\boldsymbol{y}_2'\Gamma(\boldsymbol{y}_1,\boldsymbol{y}_2)\Gamma(\boldsymbol{y}_1',\boldsymbol{y}_2') \\ & \times\mathbb{E}\big[\hat{g}_1\big(\omega_0,(\boldsymbol{x}_1,L),(\boldsymbol{y}_1,0)\big)\overline{\hat{g}_1\big(\omega_0,(\boldsymbol{x}_1,L),(\boldsymbol{y}_1',0)\big)}\big] \\ & \times\mathbb{E}\big[\overline{\hat{g}_2\big(\omega_0,(\boldsymbol{y}_3,L),(\boldsymbol{y}_2,0)\big)}\hat{g}_2\big(\omega_0,(\boldsymbol{y}_3,L),(\boldsymbol{y}_2',0)\big)\big]. \end{aligned} \tag{37}$$

Proof. Since the random media in the reference path and signal path are independent, the two functions $\hat{g}_1$ and $\hat{g}_2$ are independent, so we get from (34):

$$\begin{aligned} \mathcal{I}_{\rm gi}(\boldsymbol{x}_1) \;=\; & \frac{c_0^4}{16\omega_0^4}\int_{\mathbb{R}^2}\mathrm{d}\boldsymbol{y}_1\int_{\mathbb{R}^2}\mathrm{d}\boldsymbol{y}_1'\int_{\mathbb{R}^2}\mathrm{d}\boldsymbol{y}_2\int_{\mathbb{R}^2}\mathrm{d}\boldsymbol{y}_2'\int_{\mathbb{R}^2}\mathrm{d}\boldsymbol{y}_3\int_{\mathbb{R}^2}\mathrm{d}\boldsymbol{y}_3' \\ & \times\int_{\mathbb{R}^2}\mathrm{d}\boldsymbol{x}_2\mathbb{E}\big[\hat{g}_1\big(\omega_0,(\boldsymbol{x}_1,L),(\boldsymbol{y}_1,0)\big)\overline{\hat{g}_1\big(\omega_0,(\boldsymbol{x}_1,L),(\boldsymbol{y}_1',0)\big)}\big] \\ & \times\mathbb{E}\big[\overline{\hat{g}_2\big(\omega_0,(\boldsymbol{x}_2,L+L_0),(\boldsymbol{y}_3',L)\big)}\hat{g}_2\big(\omega_0,(\boldsymbol{x}_2,L+L_0),(\boldsymbol{y}_3,L)\big) \\ & \times\overline{\hat{g}_2\big(\omega_0,(\boldsymbol{y}_3',L),(\boldsymbol{y}_2,0)\big)}\hat{g}_2\big(\omega_0,(\boldsymbol{y}_3,L),(\boldsymbol{y}_2',0)\big)\big] \\ & \times\mathcal{T}(\boldsymbol{y}_3)\mathcal{T}(\boldsymbol{y}_3')\Gamma(\boldsymbol{y}_1,\boldsymbol{y}_2)\Gamma(\boldsymbol{y}_1',\boldsymbol{y}_2'). \end{aligned}$$

We can also use the fact that $\hat{g}_2\big(\omega_0,(\cdot,L),(\cdot,0)\big)$ and $\hat{g}_2\big(\omega_0,(\cdot,L+L_0),(\cdot,L)\big)$ are independent because they depend on $(B(\cdot,z))_{z\in[0,L]}$ and $(B(\cdot,z)-B(\cdot,L))_{z\in[L,L+L_0]}$,

respectively in Eq. (21). Therefore the ghost imaging function can be expressed as:

$$\begin{aligned}\mathcal{I}_{\rm gi}(\boldsymbol{x}_1) &= \frac{c_0^4}{16\omega_0^4}\int_{\mathbb{R}^2}\mathrm{d}\boldsymbol{y}_1\int_{\mathbb{R}^2}\mathrm{d}\boldsymbol{y}_1'\int_{\mathbb{R}^2}\mathrm{d}\boldsymbol{y}_2\int_{\mathbb{R}^2}\mathrm{d}\boldsymbol{y}_2'\int_{\mathbb{R}^2}\mathrm{d}\boldsymbol{y}_3\int_{\mathbb{R}^2}\mathrm{d}\boldsymbol{y}_3'\\ &\quad\times\int_{\mathbb{R}^2}\mathrm{d}\boldsymbol{x}_2\mathbb{E}\big[\hat{g}_1\big(\omega_0,(\boldsymbol{x}_1,L),(\boldsymbol{y}_1,0)\big)\overline{\hat{g}_1\big(\omega_0,(\boldsymbol{x}_1,L),(\boldsymbol{y}_1',0)\big)}\big]\\ &\quad\times\mathbb{E}\big[\overline{\hat{g}_2\big(\omega_0,(\boldsymbol{x}_2,L+L_0),(\boldsymbol{y}_3',L)\big)}\hat{g}_2\big(\omega_0,(\boldsymbol{x}_2,L+L_0),(\boldsymbol{y}_3,L)\big)\big]\\ &\quad\times\mathbb{E}\big[\overline{\hat{g}_2\big(\omega_0,(\boldsymbol{y}_3',L),(\boldsymbol{y}_2,0)\big)}\hat{g}_2\big(\omega_0,(\boldsymbol{y}_3,L),(\boldsymbol{y}_2',0)\big)\big]\\ &\quad\times\mathcal{T}(\boldsymbol{y}_3)\mathcal{T}(\boldsymbol{y}_3')\Gamma(\boldsymbol{y}_1,\boldsymbol{y}_2)\Gamma(\boldsymbol{y}_1',\boldsymbol{y}_2'). \end{aligned}\tag{38}$$

We denote by $\gamma_2^{(2)}$ the quantity defined by (25) and associated with the medium along the signal path (labeled ②). Using (24) and (22), we find that

$$\begin{aligned}&\int_{\mathbb{R}^2}\mathrm{d}\boldsymbol{x}_2\mathbb{E}\big[\overline{\hat{g}_2\big(\omega_0,(\boldsymbol{x}_2,L+L_0),(\boldsymbol{y}_3',L)\big)}\hat{g}_2\big(\omega_0,(\boldsymbol{x}_2,L+L_0),(\boldsymbol{y}_3,L)\big)\big]\\ &=\int_{\mathbb{R}^2}\mathrm{d}\boldsymbol{x}_2\overline{\hat{g}_0\big(\omega_0,(\boldsymbol{x}_2,L+L_0),(\boldsymbol{y}_3',L)\big)}\hat{g}_0\big(\omega_0,(\boldsymbol{x}_2,L+L_0),(\boldsymbol{y}_3,L)\big)\\ &\quad\times\exp\Big(-\frac{\gamma_2^{(2)}(\boldsymbol{y}_3'-\boldsymbol{y}_3)\omega_0^2L_0}{4c_0^2}\Big)\\ &=\frac{\omega_0^2}{4\pi^2c_0^2L_0^2}\int_{\mathbb{R}^2}\mathrm{d}\boldsymbol{x}_2\exp\Big(i\frac{\omega_0\boldsymbol{x}_2\cdot(\boldsymbol{y}_3-\boldsymbol{y}_3')}{c_0L_0}\Big)\\ &\quad\times\exp\Big(i\frac{\omega_0(|\boldsymbol{y}_3'|^2-|\boldsymbol{y}_3|^2)}{2c_0L_0}-\frac{\gamma_2^{(2)}(\boldsymbol{y}_3'-\boldsymbol{y}_3)\omega_0^2L_0}{4c_0^2}\Big)\\ &=\delta(\boldsymbol{y}_3-\boldsymbol{y}_3').\end{aligned}$$

Substituting into (38) gives the desired result. □

We will study the kernel H in the next two sections to analyze the resolution properties of ghost imaging depending on the coherence properties of the source and on the scattering properties of the random media.

7. **Resolution analysis for a fully incoherent source.** In this section we consider the fully incoherent case:

$$\Gamma(\boldsymbol{x},\boldsymbol{x}')=I_0\exp\Big(-\frac{|\boldsymbol{x}|^2}{r_0^2}\Big)\delta(\boldsymbol{x}-\boldsymbol{x}'),\tag{39}$$

in which the covariance function of the noise source is assumed to be delta-correlated and with a spatial support in the form of a Gaussian with radius r_0. The Gaussian form is useful to get explicit expressions.

Proposition 7. *In the fully incoherent case (39) the ghost imaging function is the convolution of the square transmission function with the convolution kernel $\mathcal{H}$:*

$$\mathcal{I}_{\rm gi}(\boldsymbol{x}_1)=\int_{\mathbb{R}^2}\mathcal{H}(\boldsymbol{x}_1-\boldsymbol{y}_3)\mathcal{T}(\boldsymbol{y}_3)^2\mathrm{d}\boldsymbol{y}_3,\tag{40}$$

where

$$\mathcal{H}(\boldsymbol{x})=\frac{I_0^2r_0^4}{2^9\pi^3L^4}\int_{\mathbb{R}^2}\mathrm{d}\boldsymbol{\beta}\exp\Big(-\frac{|\boldsymbol{\beta}|^2}{2}-\frac{\gamma_2(r_0\boldsymbol{\beta})\omega_0^2L}{2c_0^2}+i\frac{\omega_0r_0\boldsymbol{x}\cdot\boldsymbol{\beta}}{c_0L}\Big),\tag{41}$$

and $\gamma_2(\boldsymbol{x})=(\gamma_2^{(1)}(\boldsymbol{x})+\gamma_2^{(2)}(\boldsymbol{x}))/2$, with $\gamma_2^{(1)}$ and $\gamma_2^{(2)}$ defined as (25) and associated with the reference path (labeled ①) and signal path (labeled ②), respectively.

Proof. Using (24) we get from (37)

$$\begin{aligned} H(\boldsymbol{x}_1,\boldsymbol{y}_3) &= \frac{I_0^2 c_0^4}{16\omega_0^4}\int_{\mathbb{R}^2}\mathrm{d}\boldsymbol{y}_1\int_{\mathbb{R}^2}\mathrm{d}\boldsymbol{y}_2\exp\Big(-\frac{|\boldsymbol{y}_1|^2+|\boldsymbol{y}_2|^2}{r_0^2}\Big)\\ &\times\hat g_0\big(\omega_0,(\boldsymbol{x}_1,L),(\boldsymbol{y}_1,0)\big)\overline{\hat g_0\big(\omega_0,(\boldsymbol{x}_1,L),(\boldsymbol{y}_2,0)\big)}\\ &\quad\times\exp\Big(-\frac{\gamma_2^{(1)}(\boldsymbol{y}_1-\boldsymbol{y}_2)\omega_0^2 L}{4c_0^2}\Big)\\ &\times\overline{\hat g_0\big(\omega_0,(\boldsymbol{y}_3,L),(\boldsymbol{y}_1,0)\big)}\hat g_0\big(\omega_0,(\boldsymbol{y}_3,L),(\boldsymbol{y}_2,0)\big)\\ &\quad\times\exp\Big(-\frac{\gamma_2^{(2)}(\boldsymbol{y}_1-\boldsymbol{y}_2)\omega_0^2 L}{4c_0^2}\Big). \end{aligned}$$

Using the explicit form (22) of $\hat g_0$:

$$\begin{aligned} H(\boldsymbol{x}_1,\boldsymbol{y}_3) &= \frac{I_0^2}{16(2\pi)^4L^4}\int_{\mathbb{R}^2}\mathrm{d}\boldsymbol{y}_1\int_{\mathbb{R}^2}\mathrm{d}\boldsymbol{y}_2\exp\Big(-\frac{|\boldsymbol{y}_1|^2+|\boldsymbol{y}_2|^2}{r_0^2}\Big)\\ &\times\exp\Big(i\frac{\omega_0(\boldsymbol{y}_1-\boldsymbol{y}_2)\cdot(\boldsymbol{y}_3-\boldsymbol{x}_1)}{c_0L}\Big)\exp\Big(-\frac{\gamma_2(\boldsymbol{y}_1-\boldsymbol{y}_2)\omega_0^2L}{2c_0^2}\Big). \end{aligned}$$

By the change of variables $\boldsymbol{y}_1=\boldsymbol{x}+\boldsymbol{y}/2$, $\boldsymbol{y}_2=\boldsymbol{x}-\boldsymbol{y}/2$, and by integrating in $\boldsymbol{x}$:

$$\begin{aligned} H(\boldsymbol{x}_1,\boldsymbol{y}_3) &= \frac{I_0^2}{16(2\pi)^4L^4}\int_{\mathbb{R}^2}\mathrm{d}\boldsymbol{y}\int_{\mathbb{R}^2}\mathrm{d}\boldsymbol{x}\exp\Big(-\frac{2|\boldsymbol{x}|^2}{r_0^2}-\frac{|\boldsymbol{y}|^2}{2r_0^2}\Big)\\ &\quad\times\exp\Big(i\frac{\omega_0\boldsymbol{y}\cdot(\boldsymbol{y}_3-\boldsymbol{x}_1)}{c_0L}-\frac{\gamma_2(\boldsymbol{y})\omega_0^2L}{2c_0^2}\Big)\\ &= \frac{I_0^2r_0^2}{2^9\pi^3L^4}\int_{\mathbb{R}^2}\mathrm{d}\boldsymbol{y}\exp\Big(-\frac{|\boldsymbol{y}|^2}{2r_0^2}\Big)\\ &\quad\times\exp\Big(i\frac{\omega_0\boldsymbol{y}\cdot(\boldsymbol{y}_3-\boldsymbol{x}_1)}{c_0L}-\frac{\gamma_2(\boldsymbol{y})\omega_0^2L}{2c_0^2}\Big). \end{aligned}$$

It is therefore a function of $\boldsymbol{x}_1-\boldsymbol{y}_3$ only:

$$H(\boldsymbol{x}_1,\boldsymbol{y}_3)=\mathcal{H}(\boldsymbol{x}_1-\boldsymbol{y}_3),$$

with $\mathcal{H}(\boldsymbol{x})$ defined by (41). □

If the medium is homogeneous, $\gamma_2\equiv 0$, then the convolution kernel is Gaussian:

$$\mathcal{H}(\boldsymbol{x})=\frac{I_0^2r_0^4}{2^8\pi^2L^4}\exp\Big(-\frac{|\boldsymbol{x}|^2}{4\rho_{\mathrm{gi0}}^2}\Big), \tag{42}$$

with the radius

$$\rho_{\mathrm{gi0}}^2=\frac{c_0^2L^2}{2\omega_0^2r_0^2}. \tag{43}$$

This is essentially the classical Rayleigh resolution formula [4, Section 8.5]: ρ_{gi0} is proportional to λ_0L/r_0, with $\lambda_0=2\pi c_0/\omega_0$ the central wavelength.

If the medium is strongly scattering, in the sense that the propagation distance is larger than the scattering mean free path $L/l_{\mathrm{sca}}\gg 1$, with

$$l_{\mathrm{sca}}=\frac{8c_0^2}{\gamma_0(\mathbf{0})\omega_0^2}, \tag{44}$$

$\gamma_0(\boldsymbol{x}) = (\gamma_0^{(1)}(\boldsymbol{x}) + \gamma_0^{(2)}(\boldsymbol{x}))/2$, $\gamma_0^{(1)}$ and $\gamma_0^{(2)}$ defined as (19) and associated with the reference path (labeled ①) and signal path (labeled ②), then

$$\mathcal{H}(\boldsymbol{x}) = \frac{I_0^2 r_0^4 \rho_{\mathrm{gi0}}^2}{2^8 \pi^2 L^4 \rho_{\mathrm{gi1}}^2} \exp\Big(- \frac{|\boldsymbol{x}|^2}{4\rho_{\mathrm{gi1}}^2}\Big), \tag{45}$$

with

$$\rho_{\mathrm{gi1}}^2 = \frac{c_0^2 L^2}{2\omega_0^2 r_0^2} + \frac{4 c_0^2 L^3}{3\omega_0^2 l_{\mathrm{sca}} l_{\mathrm{cor}}^2}, \tag{46}$$

and the correlation radius of the medium l_{cor} is defined as in Proposition 3: $\gamma_0(\boldsymbol{x}) = \gamma_0(\boldsymbol{0})[1 - |\boldsymbol{x}|^2/l_{\mathrm{cor}}^2 + o(|\boldsymbol{x}|^2/l_{\mathrm{cor}}^2)]$. This result shows that the ghost imaging function still gives an image of the mask when the propagation distance is larger than the scattering mean free path, but random scattering slightly reduces its resolution. The observation that random scattering does not help comes from the fact that the two waves propagate through two independent media in the two paths. If the realizations of the random medium were identical in the two paths (which is not realistic), then random scattering would enhance the resolution, as we explain in Appendix D and as we observed in time-reversal experiments [3, 7, 8].

8. **Resolution analysis for a partially coherent source.** In this section we consider the partially coherent case:

$$\Gamma(\boldsymbol{x}, \boldsymbol{x}') = I_0 \exp\Big(- \frac{|\boldsymbol{x} + \boldsymbol{x}'|^2}{4r_0^2} - \frac{|\boldsymbol{x} - \boldsymbol{x}'|^2}{4\rho_0^2}\Big), \tag{47}$$

in which the source is assumed to have a spatial support in the form of a Gaussian with radius r_0 and a local Gaussian correlation function with radius ρ_0. This model is called Gaussian-Schell in the physical literature [19]. Note that we always have $r_0 \geq \rho_0$ (to ensure that Γ is a positive kernel). The limit case $\rho_0 \to 0$ corresponds to the fully incoherent situation addressed in the previous section. The limit case $\rho_0 = r_0$ in which

$$\Gamma(\boldsymbol{x}, \boldsymbol{x}') = I_0 \exp\Big(- \frac{|\boldsymbol{x}|^2}{2r_0^2} - \frac{|\boldsymbol{x}'|^2}{2r_0^2}\Big)$$

corresponds to the fully coherent situation: the spatial profile of the field is deterministic and has a Gaussian form with radius r_0. The following proposition gives the expression of the ghost imaging kernel.

Proposition 8. *In the partially coherent case (47) the ghost imaging function has the form (36) with the imaging kernel given by*

$$\begin{aligned} H(\boldsymbol{x}_1, \boldsymbol{y}_3) = {} & \frac{I_0^2 \rho_0^4 r_0^4}{64\pi^2 L^4} \int_{\mathbb{R}^2} \mathrm{d}\boldsymbol{\alpha} \int_{\mathbb{R}^2} \mathrm{d}\boldsymbol{\beta} \exp\Big(- \frac{|\boldsymbol{\alpha}|^2 + |\boldsymbol{\beta}|^2}{2}\big(1 + \frac{\omega_0^2 r_0^2 \rho_0^2}{c_0^2 L^2}\big)\Big) \\ & \times \exp\Big(- i \frac{\omega_0}{c_0 L}\big(\rho_0(\boldsymbol{x}_1 + \boldsymbol{y}_3)\cdot\boldsymbol{\alpha} + r_0(\boldsymbol{x}_1 - \boldsymbol{y}_3)\cdot\boldsymbol{\beta}\big)\Big) \\ & \times \exp\Big(- \frac{\omega_0^2 L}{4c_0^2}\big(\gamma_2^{(1)}(\rho_0\boldsymbol{\alpha} + r_0\boldsymbol{\beta}) + \gamma_2^{(2)}(\rho_0\boldsymbol{\alpha} - r_0\boldsymbol{\beta})\big)\Big). \end{aligned} \tag{48}$$

Proof. We have from (37) and the form (47) of the covariance function Γ:

$$
\begin{aligned}
H(\boldsymbol{x}_1,\boldsymbol{y}_3) = {} & \frac{I_0^2}{2^8\pi^4 L^4}\int_{\mathbb{R}^2}\mathrm{d}\boldsymbol{y}_1\int_{\mathbb{R}^2}\mathrm{d}\boldsymbol{y}_1'\int_{\mathbb{R}^2}\mathrm{d}\boldsymbol{y}_2\int_{\mathbb{R}^2}\mathrm{d}\boldsymbol{y}_2' \\
& \times\exp\Big(-\frac{|\boldsymbol{y}_1+\boldsymbol{y}_2|^2}{4r_0^2}-\frac{|\boldsymbol{y}_1-\boldsymbol{y}_2|^2}{4\rho_0^2}-\frac{|\boldsymbol{y}_1'+\boldsymbol{y}_2'|^2}{4r_0^2}-\frac{|\boldsymbol{y}_1'-\boldsymbol{y}_2'|^2}{4\rho_0^2}\Big) \\
& \times\exp\Big(i\frac{\omega_0}{c_0L}\big(\boldsymbol{x}_1\cdot(\boldsymbol{y}_1'-\boldsymbol{y}_1)+\boldsymbol{y}_3\cdot(\boldsymbol{y}_2-\boldsymbol{y}_2')\big)\Big) \\
& \times\exp\Big(i\frac{\omega_0}{2c_0L}\big(|\boldsymbol{y}_1|^2-|\boldsymbol{y}_1'|^2+|\boldsymbol{y}_2'|^2-|\boldsymbol{y}_2|^2\big)\Big) \\
& \times\exp\Big(-\frac{\omega_0^2L}{4c_0^2}\big(\gamma_2^{(2)}(\boldsymbol{y}_2-\boldsymbol{y}_2')+\gamma_2^{(1)}(\boldsymbol{y}_1'-\boldsymbol{y}_1)\big)\Big).
\end{aligned}
$$

After the change of variables

$$
\boldsymbol{x}_a=\frac{\boldsymbol{y}_1+\boldsymbol{y}_1'}{2},\quad \boldsymbol{y}_a=\boldsymbol{y}_1-\boldsymbol{y}_1',\quad \boldsymbol{x}_b=\frac{\boldsymbol{y}_2+\boldsymbol{y}_2'}{2},\quad \boldsymbol{y}_b=\boldsymbol{y}_2'-\boldsymbol{y}_2,
$$

H can be written as

$$
\begin{aligned}
H(\boldsymbol{x}_1,\boldsymbol{y}_3) = {} & \frac{I_0^2}{2^8\pi^4 L^4}\int_{\mathbb{R}^2}\mathrm{d}\boldsymbol{x}_a\int_{\mathbb{R}^2}\mathrm{d}\boldsymbol{x}_b\int_{\mathbb{R}^2}\mathrm{d}\boldsymbol{y}_a\int_{\mathbb{R}^2}\mathrm{d}\boldsymbol{y}_b \\
& \times\exp\Big(-\frac{|\boldsymbol{x}_a+\boldsymbol{x}_b|^2}{2r_0^2}-\frac{|\boldsymbol{x}_a-\boldsymbol{x}_b|^2}{2\rho_0^2}-\frac{|\boldsymbol{y}_a-\boldsymbol{y}_b|^2}{8r_0^2}-\frac{|\boldsymbol{y}_a+\boldsymbol{y}_b|^2}{8\rho_0^2}\Big) \\
& \times\exp\Big(i\frac{\omega_0}{c_0L}\big((\boldsymbol{x}_a-\boldsymbol{x}_1)\cdot\boldsymbol{y}_a+(\boldsymbol{x}_b-\boldsymbol{y}_3)\cdot\boldsymbol{y}_b\big)\Big) \\
& \times\exp\Big(-\frac{\omega_0^2L}{4c_0^2}\big(\gamma_2^{(2)}(\boldsymbol{y}_b)+\gamma_2^{(1)}(\boldsymbol{y}_a)\big)\Big).
\end{aligned}
$$

After integration in $\boldsymbol{x}_a$ and $\boldsymbol{x}_b$, we get

$$
\begin{aligned}
H(\boldsymbol{x}_1,\boldsymbol{y}_3) = {} & \frac{I_0^2r_0^2\rho_0^2}{2^8\pi^2 L^4}\int_{\mathbb{R}^2}\mathrm{d}\boldsymbol{y}_a\int_{\mathbb{R}^2}\mathrm{d}\boldsymbol{y}_b \\
& \times\exp\Big(-\frac{|\boldsymbol{y}_a-\boldsymbol{y}_b|^2}{8r_0^2}-\frac{|\boldsymbol{y}_a+\boldsymbol{y}_b|^2}{8\rho_0^2}-i\frac{\omega_0}{c_0L}\big(\boldsymbol{y}_a\cdot\boldsymbol{x}_1+\boldsymbol{y}_b\cdot\boldsymbol{y}_3\big)\Big) \\
& \times\exp\Big(-\frac{\omega_0^2}{8c_0^2L^2}\big(r_0^2|\boldsymbol{y}_a+\boldsymbol{y}_b|^2+\rho_0^2|\boldsymbol{y}_a-\boldsymbol{y}_b|^2\big)\Big) \\
& \times\exp\Big(-\frac{\omega_0^2L}{4c_0^2}\big(\gamma_2^{(2)}(\boldsymbol{y}_b)+\gamma_2^{(1)}(\boldsymbol{y}_a)\big)\Big).
\end{aligned}
$$

We get the expression (48) after the new change of variables $\boldsymbol{y}_a=\rho_0\boldsymbol{\alpha}+r_0\boldsymbol{\beta}$ and $\boldsymbol{y}_b=\rho_0\boldsymbol{\alpha}-r_0\boldsymbol{\beta}$. □

If the medium is homogeneous along the two paths $\gamma_0^{(1)}=\gamma_0^{(2)}=0$, then the imaging kernel is

$$
H(\boldsymbol{x}_1,\boldsymbol{y}_3)=\frac{I_0^2\rho_0^2r_0^2c_0^4}{64\omega_0^4\rho_{\mathrm{gi}}^2R_{\mathrm{gi}}^2}\exp\Big(-\frac{|\boldsymbol{x}_1-\boldsymbol{y}_3|^2}{4\rho_{\mathrm{gi2}}^2}-\frac{|\boldsymbol{x}_1+\boldsymbol{y}_3|^2}{4R_{\mathrm{gi2}}^2}\Big), \tag{49}
$$

with

$$\rho_{\rm gi2}^2 = \frac{c_0^2 L^2}{2\omega_0^2 r_0^2} + \frac{\rho_0^2}{2}, \tag{50}$$

$$R_{\rm gi2}^2 = \frac{c_0^2 L^2}{2\omega_0^2 \rho_0^2} + \frac{r_0^2}{2}. \tag{51}$$

By comparing with (43), Eq. (50) shows that the partial coherence of the source reduces the resolution of the ghost imaging function, while Eq. (51) shows that it also reduces the diameter of the region that can be imaged.

If the medium is random along the two paths and the statistics of the random media along the reference and signal paths are identical (they are two independent realizations of the same process), then $\gamma_0^{(2)} = \gamma_0^{(1)} = \gamma_0$. When scattering is strong, in the sense that the propagation distance is larger than the scattering mean free path $L/l_{\rm sca} \gg 1$, with $l_{\rm sca}$ given by (44), then

$$H(\boldsymbol{x}_1, \boldsymbol{y}_3) = \frac{I_0^2 \rho_0^2 r_0^2 c_0^4}{64\omega_0^4 \rho_{\rm gi}^2 R_{\rm gi}^2} \exp\Big(- \frac{|\boldsymbol{x}_1 - \boldsymbol{y}_3|^2}{4\rho_{\rm gi}^2} - \frac{|\boldsymbol{x}_1 + \boldsymbol{y}_3|^2}{4R_{\rm gi}^2}\Big), \tag{52}$$

with

$$\rho_{\rm gi}^2 = \frac{c_0^2 L^2}{2\omega_0^2 r_0^2} + \frac{\rho_0^2}{2} + \frac{4c_0^2 L^3}{3\omega_0^2 l_{\rm sca} l_{\rm cor}^2}, \tag{53}$$

$$R_{\rm gi}^2 = \frac{c_0^2 L^2}{2\omega_0^2 \rho_0^2} + \frac{r_0^2}{2} + \frac{4c_0^2 L^3}{3\omega_0^2 l_{\rm sca} l_{\rm cor}^2}, \tag{54}$$

and the correlation radius of the medium $l_{\rm cor}$ is defined as in Proposition 3: $\gamma_0(\boldsymbol{x}) = \gamma_0(\boldsymbol{0})[1 - |\boldsymbol{x}|^2/l_{\rm cor}^2 + o(|\boldsymbol{x}|^2/l_{\rm cor}^2)]$. These formulas also give the expression (49) of the imaging kernel when the medium is homogeneous: it suffices to take $l_{\rm sca} \to \infty$.

In the partially coherent case $\rho_0 \le r_0$, formula (53) shows that the resolution is reduced by the spatial coherence of the source. Formula (54) also shows that imaging is possible provided the object to be imaged (i.e. the support of the transmission function) is within the disk with radius $R_{\rm gi}$. This radius is all the larger as the source is less coherent, but it increases when scattering becomes stronger. In other words, scattering reduces the resolution of the ghost imaging function, but it increases the diameter of the region that can be imaged.

In the limit case of a fully incoherent source $\rho_0 \to 0$, we recover the result of the previous section. More exactly we have

$$\frac{1}{4\pi\rho_0^2}\Gamma(\boldsymbol{x}, \boldsymbol{x}') \overset{\rho_0 \to 0}{\longrightarrow} I_0 \exp\Big(- \frac{|\boldsymbol{x}|^2}{r_0^2}\Big)\delta(\boldsymbol{x} - \boldsymbol{x}')$$

and

$$\frac{1}{(4\pi\rho_0^2)^2} H(\boldsymbol{x}_1, \boldsymbol{y}_3) \overset{\rho_0 \to 0}{\longrightarrow} \frac{I_0^2 r_0^4 \rho_{\rm gi0}^2}{2^8 \pi^2 L^4 \rho_{\rm gi1}^2} \exp\Big(- \frac{|\boldsymbol{x}_1 - \boldsymbol{y}_3|^2}{4\rho_{\rm gi1}^2}\Big),$$

as in (45). The formulas (53) and (54) give the conditions under which the fully incoherent approximation is valid: it is possible to approximate the partially coherent case (47) by the fully incoherent case (39) when ρ_0 is small enough so that ρ_0 is much smaller than $\rho_{\rm gi0}$ and the support of the transmission function is within the disk with radius $\rho_{\rm gi0} r_0/\rho_0$ (or more exactly $\sqrt{\rho_{\rm gi0}^2 r_0^2/\rho_0^2 + 4c_0^2 L^3/(3\omega_0^2 l_{\rm sca} l_{\rm cor}^2)}$).

In the limit case of a fully coherent source $\rho_0 = r_0$, then $\rho_{\rm gi}^2 = R_{\rm gi}^2$ and

$$H(\boldsymbol{x}_1, \boldsymbol{y}_3) = \frac{I_0^2 r_0^4 c_0^4}{64\omega_0^4 R_{\rm gi}^4} \exp\Big(- \frac{|\boldsymbol{x}_1|^2}{2R_{\rm gi}^2} - \frac{|\boldsymbol{y}_3|^2}{2R_{\rm gi}^2}\Big),$$

which has a separable form. In this case we do not get any image of the transmission function and the imaging function has a Gaussian form with width $R_{\rm gi}$ whatever the form of the transmission function. This confirms that the incoherence (or partial coherence) of the source is the key ingredient for ghost imaging.

To summarize: the ghost imaging function can exploit the partial coherence of the source because the same source illuminates both paths. It cannot exploit the incoherence induced by scattering because the two paths are occupied by two different realizations of the random medium.

9. **Concluding remarks.** In this paper we have addressed transmission-based ghost imaging. It is also possible to address reflective ghost imaging, in order to image rough-surfaced targets in reflection [14, 21]. Moreover, refined versions of ghost imaging can be found in the literature. A first proposition is that it is not required to measure the complete transmitted intensity of the reference field and that the number of measurements required for image recovery can be reduced if an advanced reconstruction algorithm based on compressive sensing is used [17]. A second proposition is that there is no need for the high-resolution detector at all if the partially coherent source can be perfectly controlled. For instance, if the source is generated by a spatial light modulator, then the reference field can be computed (assuming a homogeneous medium) instead of being measured, and then the ghost imaging function is the correlation of the measured spatially-integrated intensity of the signal field at the bucket detector with the computed intensity of the reference field [20]. It is remarkable that in this configuration, a high-resolution image of the object can be obtained with only one bucket (single-pixel) detector.

Appendix A. **The signal and reference fields in the white-noise paraxial regime.** In this appendix we describe the signal wave v_2^ε in the plane of the bucket detector and the reference wave v_1^ε in the plane of the high-resolution detector in the paraxial regime. They are expressed in terms of the fundamental functions $\hat{g}_1$ and $\hat{g}_2$ of the random medium along the reference path (labeled ①) and the signal path (labeled ②) defined in (21).

The slowly varying envelope of the reference wave in the plane of the high-resolution detector $z = L$ at a point $\vec{\boldsymbol{x}}_1^\varepsilon = (\varepsilon^2 \boldsymbol{x}_1, L)$ is

$$\hat{v}_1^\varepsilon(\omega, \vec{\boldsymbol{x}}_1^\varepsilon) = \int_{\mathbb{R}^2} \hat{\mathcal{G}}_1^\varepsilon\big(\frac{\omega_0}{\varepsilon^4} + \omega, \vec{\boldsymbol{x}}_1^\varepsilon, (\boldsymbol{x}_s, 0)\big) \hat{f}^\varepsilon(\omega, \boldsymbol{x}_s) \mathrm{d}\boldsymbol{x}_s,$$

where $\hat{\mathcal{G}}_1^\varepsilon = \hat{G}_1^\varepsilon$ is the Green's function of the random medium in the reference path and the source term in the paraxial regime is

$$\hat{f}^\varepsilon(\omega, \boldsymbol{x}_s) = \varepsilon^p \hat{f}\Big(\varepsilon^p \omega, \frac{\boldsymbol{x}_s}{\varepsilon^2}\Big).$$

In terms of the paraxial fundamental solution this reads

$$\begin{aligned}\hat{v}_1^\varepsilon\Big(\frac{\omega}{\varepsilon^p},\vec{\boldsymbol{x}}_1^\varepsilon\Big) &= \varepsilon^{4+p}\int_{\mathbb{R}^2}\hat{G}_1^\varepsilon\Big(\frac{\omega_0}{\varepsilon^4}+\frac{\omega}{\varepsilon^p},(\varepsilon^2\boldsymbol{x}_1,L),(\varepsilon^2\boldsymbol{x}_s,0)\Big)\hat{f}(\omega,\boldsymbol{x}_s)\mathrm{d}\boldsymbol{x}_s\\ &\xrightarrow{\varepsilon\to 0} \frac{ic_0\varepsilon^{4+p}}{2\omega_0}\exp\Big(i\big(\frac{\omega_0}{\varepsilon^4}+\frac{\omega}{\varepsilon^p}\big)\frac{L}{c_0}\Big)\\ &\quad\times\int_{\mathbb{R}^2}\hat{g}_1\big(\omega_0,(\boldsymbol{x}_1,L),(\boldsymbol{x}_s,0)\big)\hat{f}(\omega,\boldsymbol{x}_s)\mathrm{d}\boldsymbol{x}_s.\end{aligned}$$

Here we have used the fact that, when $p<4$, the paraxial fundamental solution $\hat{g}_1\big(\omega_0+\varepsilon^{4-p}\omega,(\boldsymbol{x}_1,L),(\boldsymbol{x}_s,0)\big)$ does not depend on ω and it is equal to its value at the central frequency ω_0, as shown in [12, Section 4.1].

The slowly varying envelope of the signal wave in the plane of the bucket detector $z=L+L_0$ at a point $\vec{\boldsymbol{x}}_2^\varepsilon=(\varepsilon^2\boldsymbol{x}_2,L+L_0)$ is

$$\hat{v}_2^\varepsilon(\omega,\vec{\boldsymbol{x}}_2^\varepsilon)=\int_{\mathbb{R}^2}\hat{\mathcal{G}}_2^\varepsilon\big(\frac{\omega_0}{\varepsilon^4}+\omega,\vec{\boldsymbol{x}}_2^\varepsilon,(\boldsymbol{x}_s,0)\big)\hat{f}^\varepsilon(\omega,\boldsymbol{x}_s)\mathrm{d}\boldsymbol{x}_s.$$

Here

$$\begin{aligned}&\hat{\mathcal{G}}_2^\varepsilon\big(\omega,\vec{\boldsymbol{x}}_2^\varepsilon,(\boldsymbol{x}_s,0)\big)\\ &=-\frac{2i\omega}{c_0}\int_{\mathbb{R}^2}\hat{G}_2^\varepsilon\big(\omega,\vec{\boldsymbol{x}}_2^\varepsilon,(\boldsymbol{y},L)\big)\mathcal{T}^\varepsilon(\boldsymbol{y})\hat{G}_2^\varepsilon\big(\omega,(\boldsymbol{y},L),(\boldsymbol{x}_s,0)\big)\mathrm{d}\boldsymbol{y},\end{aligned}$$

where $\hat{G}_2^\varepsilon$ is the Green's function of the random medium in the signal path and $\mathcal{T}^\varepsilon(\boldsymbol{y})=\mathcal{T}(\boldsymbol{y}/\varepsilon^2)$ is the transmission function that models the object to be imaged. Therefore we can also write

$$\hat{v}_2^\varepsilon\Big(\frac{\omega}{\varepsilon^p},\vec{\boldsymbol{x}}_2^\varepsilon\Big)=\varepsilon^{4+p}\int_{\mathbb{R}^2}\hat{\mathcal{G}}_2^\varepsilon\Big(\frac{\omega_0}{\varepsilon^4}+\frac{\omega}{\varepsilon^p},\vec{\boldsymbol{x}}_2^\varepsilon,(\varepsilon^2\boldsymbol{x}_s,0)\Big)\hat{f}(\omega,\boldsymbol{x}_s)\mathrm{d}\boldsymbol{x}_s,$$

with

$$\begin{aligned}\hat{\mathcal{G}}_2^\varepsilon\Big(\frac{\omega_0}{\varepsilon^4}+\frac{\omega}{\varepsilon^p},\vec{\boldsymbol{x}}_2^\varepsilon,(\varepsilon^2\boldsymbol{x}_s,0)\Big) &= -\frac{2i(\omega_0+\varepsilon^{4-p}\omega)}{c_0}\int_{\mathbb{R}^2}\hat{G}_2^\varepsilon\big(\frac{\omega_0}{\varepsilon^4}+\frac{\omega}{\varepsilon^p},\vec{\boldsymbol{x}}_2^\varepsilon,(\varepsilon^2\boldsymbol{y},L)\big)\\ &\quad\times\mathcal{T}(\boldsymbol{y})\hat{G}_2^\varepsilon\big(\frac{\omega_0}{\varepsilon^4}+\frac{\omega}{\varepsilon^p},(\varepsilon^2\boldsymbol{y},L),(\varepsilon^2\boldsymbol{x}_s,0)\big)\mathrm{d}\boldsymbol{y}.\end{aligned}$$

In terms of the paraxial fundamental solutions this reads

$$\begin{aligned}\hat{v}_2^\varepsilon\Big(\frac{\omega}{\varepsilon^p},\vec{\boldsymbol{x}}_2^\varepsilon\Big) &\xrightarrow{\varepsilon\to 0} \frac{ic_0\varepsilon^{4+p}}{2\omega_0}\exp\Big(i\big(\frac{\omega_0}{\varepsilon^4}+\frac{\omega}{\varepsilon^p}\big)\frac{L+L_0}{c_0}\Big)\\ &\quad\times\int_{\mathbb{R}^2}\int_{\mathbb{R}^2}\hat{g}_2\big(\omega_0,(\boldsymbol{x}_2,L+L_0),(\boldsymbol{y},L)\big)\\ &\quad\times\mathcal{T}(\boldsymbol{y})\hat{g}_2\big(\omega_0,(\boldsymbol{y},L),(\boldsymbol{x}_s,0)\big)\hat{f}(\omega,\boldsymbol{x}_s)\mathrm{d}\boldsymbol{x}_s\mathrm{d}\boldsymbol{y}.\end{aligned}$$

Appendix B. **Proof of Proposition 2.** Let us fix ω and skip it in the notations. Let us consider the solution to (20) with an arbitrary initial condition $\hat{\phi}(\boldsymbol{x},z=0)=\hat{\phi}_{\mathrm{ic}}(\boldsymbol{x})$. The first-order moment

$$M_1(\boldsymbol{x},z)=\mathbb{E}\big[\hat{\phi}(\boldsymbol{x},z)\big] \tag{55}$$

satisfies the Schrödinger equation with homogeneous damping:

$$\frac{\partial M_1}{\partial z}=\frac{ic_0}{2\omega}\Delta_{\boldsymbol{x}}M_1-\frac{\omega^2\gamma_0(\boldsymbol{0})}{8c_0^2}M_1, \tag{56}$$

$$M_1(\boldsymbol{x},z=0)=\hat{\phi}_{\mathrm{ic}}(\boldsymbol{x}). \tag{57}$$

The solution can be obtained by taking a Fourier transform in $\boldsymbol{x}$, solving the equation for the Fourier transform, and taking an inverse Fourier transform:

$$M_1(\boldsymbol{x},z)=\frac{1}{4\pi^2}\int_{\mathbb{R}^2}\mathrm{d}\boldsymbol{\kappa}\check{\phi}_{\rm ic}(\boldsymbol{\kappa})\exp\Big(i\boldsymbol{\kappa}\cdot\boldsymbol{x}-\frac{ic_0|\boldsymbol{\kappa}|^2}{2\omega}z-\frac{\omega^2\gamma_0(\mathbf{0})}{8c_0^2}z\Big), \tag{58}$$

with

$$\check{\phi}_{\rm ic}(\boldsymbol{\kappa})=\int_{\mathbb{R}^2}\hat{\phi}_{\rm ic}(\boldsymbol{x})\exp\big(-i\boldsymbol{\kappa}\cdot\boldsymbol{x}\big)\mathrm{d}\boldsymbol{x}.$$

In particular, if the input spatial profile is Gaussian with radius $r_{\rm ic}$ and unit L^1-norm:

$$\hat{\phi}_{\rm ic}(\boldsymbol{x})=\frac{1}{2\pi r_{\rm ic}^2}\exp\Big(-\frac{|\boldsymbol{x}|^2}{2r_{\rm ic}^2}\Big), \tag{59}$$

then

$$M_1(\boldsymbol{x},z)=\frac{1}{2\pi(r_{\rm ic}^2+\frac{ic_0z}{\omega})}\exp\Big(-\frac{|\boldsymbol{x}|^2}{2(r_{\rm ic}^2+\frac{ic_0z}{\omega})}\Big)\exp\Big(-\frac{\omega^2\gamma_0(\mathbf{0})}{8c_0^2}z\Big). \tag{60}$$

If the initial condition is a point-like source with unit amplitude (which can be viewed as a limit of the Gaussian initial condition (59) in which $r_{\rm ic}\to 0$), then

$$M_1(\boldsymbol{x},z)=\frac{\omega}{2i\pi c_0z}\exp\Big(i\frac{\omega|\boldsymbol{x}|^2}{2c_0z}\Big)\exp\Big(-\frac{\omega^2\gamma_0(\mathbf{0})}{8c_0^2}z\Big), \tag{61}$$

as stated in the proposition in (23).

By applying Itô's formula to (20) the second-order moments

$$M_2(\boldsymbol{x},\boldsymbol{x}',z)=\mathbb{E}\big[\hat{\phi}(\boldsymbol{x},z)\overline{\hat{\phi}(\boldsymbol{x}',z)}\big] \tag{62}$$

satisfy the system:

$$\frac{\partial M_2}{\partial z}=\frac{ic_0}{2\omega}\big(\Delta_{\boldsymbol{x}}-\Delta_{\boldsymbol{x}'}\big)M_2+\frac{\omega_0^2}{4c_0^2}\big(\gamma_0(\boldsymbol{x}-\boldsymbol{x}')-\gamma_0(\mathbf{0})\big)M_2, \tag{63}$$

$$M_2(\boldsymbol{x},\boldsymbol{x}',z=0)=\hat{\phi}_{\rm ic}(\boldsymbol{x})\overline{\hat{\phi}_{\rm ic}(\boldsymbol{x}')}. \tag{64}$$

A convenient approach for solving the second-order moment equation is via the Wigner transform. The Wigner transform of the field is defined by

$$W(\boldsymbol{x},\boldsymbol{q},z)=\int_{\mathbb{R}^2}\exp\big(-i\boldsymbol{q}\cdot\boldsymbol{y}\big)\mathbb{E}\Big[\hat{\phi}\big(\boldsymbol{x}+\frac{\boldsymbol{y}}{2},z\big)\overline{\hat{\phi}}\big(\boldsymbol{x}-\frac{\boldsymbol{y}}{2},z\big)\Big]\,\mathrm{d}\boldsymbol{y}. \tag{65}$$

Using (63) and defining

$$\check{\gamma}_0(\boldsymbol{\kappa})=\int_{\mathbb{R}^2}\gamma_0(\boldsymbol{x})\exp(-i\boldsymbol{\kappa}\cdot\boldsymbol{x})\mathrm{d}\boldsymbol{x},$$

we find that it satisfies the closed system

$$\frac{\partial W}{\partial z}+\frac{c_0}{\omega}\boldsymbol{q}\cdot\nabla_{\boldsymbol{x}}W=\frac{\omega^2}{16\pi^2c_0^2}\int_{\mathbb{R}^2}\check{\gamma}_0(\boldsymbol{\kappa})\Big[W(\boldsymbol{q}-\boldsymbol{\kappa})-W(\boldsymbol{q})\Big]\mathrm{d}\boldsymbol{\kappa}, \tag{66}$$

starting from $W(\boldsymbol{x},\boldsymbol{q},z=0)=W_{\rm ic}(\boldsymbol{x},\boldsymbol{q})$, which is the Wigner transform of the initial field $\hat{\phi}_{\rm ic}$:

$$W_{\rm ic}(\boldsymbol{x},\boldsymbol{q})=\int_{\mathbb{R}^2}\exp\big(-i\boldsymbol{q}\cdot\boldsymbol{y}\big)\hat{\phi}_{\rm ic}\big(\boldsymbol{x}+\frac{\boldsymbol{y}}{2}\big)\overline{\hat{\phi}_{\rm ic}}\big(\boldsymbol{x}-\frac{\boldsymbol{y}}{2}\big)\mathrm{d}\boldsymbol{y}.$$

Eq. (66) has the form of a radiative transport equation for the angularly-resolved wave energy density W. In this context $\omega^2\gamma_0(\mathbf{0})/(4c_0^2)$ is the total scattering cross-section and $\omega^2\hat{\gamma}_0(\cdot)/(16\pi^2c_0^2)$ is the differential scattering cross-section that gives the mode conversion rate.

By taking a Fourier transform in $\boldsymbol{q}$ and $\boldsymbol{x}$ of Eq. (66), we obtain a transport equation that can be integrated and we find the following integral representation for W:

$$\begin{aligned} W(\boldsymbol{x},\boldsymbol{q},z) &= \frac{1}{4\pi^2}\iint_{\mathbb{R}^2\times\mathbb{R}^2}\exp\Big(i\boldsymbol{\xi}\cdot(\boldsymbol{x}-\boldsymbol{q}\frac{c_0z}{\omega})-i\boldsymbol{y}\cdot\boldsymbol{q}\Big)\hat{W}_{\rm ic}(\boldsymbol{\xi},\boldsymbol{y}) \\ &\quad\times\exp\Big(\frac{\omega^2}{4c_0^2}\int_0^z\gamma_0(\boldsymbol{y}+\boldsymbol{\xi}\frac{c_0z'}{\omega})-\gamma_0(\mathbf{0})\mathrm{d}z'\Big)\mathrm{d}\boldsymbol{\xi}\mathrm{d}\boldsymbol{y}, \end{aligned} \tag{67}$$

where $\hat{W}_{\rm ic}$ is associated to the initial field $\hat{\phi}_{\rm ic}$:

$$\hat{W}_{\rm ic}(\boldsymbol{\xi},\boldsymbol{y})=\int_{\mathbb{R}^2}\exp\big(-i\boldsymbol{\xi}\cdot\boldsymbol{x}\big)\hat{\phi}_{\rm ic}\big(\boldsymbol{x}+\frac{\boldsymbol{y}}{2}\big)\overline{\hat{\phi}_{\rm ic}}\big(\boldsymbol{x}-\frac{\boldsymbol{y}}{2}\big)\mathrm{d}\boldsymbol{x}.$$

By taking an inverse Fourier transform the expression (67) can indeed be used to compute and discuss the mutual coherence function:

$$\begin{aligned} \Gamma^{(2)}(\boldsymbol{x},\boldsymbol{y},z) &= M_2\Big(\boldsymbol{x}+\frac{\boldsymbol{y}}{2},\boldsymbol{x}-\frac{\boldsymbol{y}}{2},z\Big) \\ &= \mathbb{E}\Big[\hat{\phi}\Big(\boldsymbol{x}+\frac{\boldsymbol{y}}{2},z\Big)\overline{\hat{\phi}}\Big(\boldsymbol{x}-\frac{\boldsymbol{y}}{2},z\Big)\Big] \end{aligned} \tag{68}$$

is given by

$$\begin{aligned} \Gamma^{(2)}(\boldsymbol{x},\boldsymbol{y},z) &= \frac{1}{4\pi^2}\int_{\mathbb{R}^2}\exp\big(i\boldsymbol{\xi}\cdot\boldsymbol{x}\big)\hat{W}_{\rm ic}\big(\boldsymbol{\xi},\boldsymbol{y}-\boldsymbol{\xi}\frac{c_0z}{\omega}\big) \\ &\quad\times\exp\Big(\frac{\omega^2}{4c_0^2}\int_0^z\gamma_0\big(\boldsymbol{y}-\boldsymbol{\xi}\frac{c_0z'}{\omega}\big)-\gamma_0(\mathbf{0})\mathrm{d}z'\Big)\mathrm{d}\boldsymbol{\xi}, \end{aligned} \tag{69}$$

where $\boldsymbol{x}$ is the mid-point and $\boldsymbol{y}$ is the offset. Let us examine two particular initial conditions, which corresponds to a Gaussian-beam wave and to a point-like source, respectively.

If the input spatial profile is Gaussian with radius $r_{\rm ic}$ and unit norm as in (59), then we have

$$\hat{W}_{\rm ic}(\boldsymbol{\xi},\boldsymbol{y})=\frac{1}{4\pi r_{\rm ic}^2}\exp\Big(-\frac{r_{\rm ic}^2|\boldsymbol{\xi}|^2}{4}-\frac{|\boldsymbol{y}|^2}{4r_{\rm ic}^2}\Big), \tag{70}$$

and we find from (69) that the second-order moment of the field has the form

$$\begin{aligned} \Gamma^{(2)}(\boldsymbol{x},\boldsymbol{y},z) &= \frac{1}{16\pi^3r_{\rm ic}^2}\int_{\mathbb{R}^2}\exp\Big(-\frac{1}{4r_{\rm ic}^2}\big|\boldsymbol{y}-\boldsymbol{\xi}\frac{c_0z}{\omega}\big|^2-\frac{r_{\rm ic}^2|\boldsymbol{\xi}|^2}{4}+i\boldsymbol{\xi}\cdot\boldsymbol{x}\Big) \\ &\quad\times\exp\Big(\frac{\omega^2}{4c_0^2}\int_0^z\gamma_0\big(\boldsymbol{y}-\boldsymbol{\xi}\frac{c_0z'}{\omega}\big)-\gamma_0(\mathbf{0})\mathrm{d}z'\Big)\mathrm{d}\boldsymbol{\xi}. \end{aligned} \tag{71}$$

If the initial condition is a point-like source with unit amplitude (which can be viewed as a limit of the Gaussian initial condition in which $r_{\rm ic}\to 0$), then $\hat{W}_{\rm ic}(\boldsymbol{\xi},\boldsymbol{y})=\delta(\boldsymbol{y})$ and

$$\begin{aligned} \Gamma^{(2)}(\boldsymbol{x},\boldsymbol{y},z) &= \frac{\omega^2}{4\pi^2c_0^2z^2}\exp\Big(\frac{i\omega}{c_0z}\boldsymbol{y}\cdot\boldsymbol{x}\Big) \\ &\quad\times\exp\Big(\frac{\omega^2}{4c_0^2}\int_0^z\big(\gamma_0(\boldsymbol{y}\frac{z'}{z})-\gamma_0(\mathbf{0})\big)\mathrm{d}z'\Big), \end{aligned} \tag{72}$$

which gives the desired result (24).

Appendix C. Proof of Proposition 4. We consider that the initial condition is (30) and we use the same notations as in the previous appendix. We have

$$\hat{W}_{\rm ic}(\boldsymbol{\xi},\boldsymbol{y}) = \pi r_{\rm ic}^2 \exp\Big(-\frac{r_{\rm ic}^2|\boldsymbol{\xi}|^2}{4} - \frac{|\boldsymbol{y}|^2}{4r_{\rm ic}^2}\Big),$$

and we find from (69) that the second-order moment of the field has the form

$$\begin{aligned}\Gamma^{(2)}(\boldsymbol{x},\boldsymbol{y},z) &= \frac{r_{\rm ic}^2}{4\pi}\int_{\mathbb{R}^2}\exp\Big(-\frac{1}{4r_{\rm ic}^2}\big|\boldsymbol{y}-\boldsymbol{\xi}\frac{c_0 z}{\omega}\big|^2 - \frac{r_{\rm ic}^2|\boldsymbol{\xi}|^2}{4} + i\boldsymbol{\xi}\cdot\boldsymbol{x}\Big)\\ &\quad\times\exp\Big(\frac{\omega^2}{4c_0^2}\int_0^z \gamma_0\big(\boldsymbol{y}-\boldsymbol{\xi}\frac{c_0 z'}{\omega}\big) - \gamma_0(\boldsymbol{0})\mathrm{d}z'\Big)\mathrm{d}\boldsymbol{\xi}. \qquad (73)\end{aligned}$$

In the strongly scattering regime $z \gg l_{\rm sca}$ we can use the expansion $\gamma_0(\boldsymbol{x}) = \gamma_0(\boldsymbol{0})[1 - |\boldsymbol{x}|^2/l_{\rm cor}^2 + o(|\boldsymbol{x}|^2/l_{\rm cor}^2)]$ in the exponent term

$$\exp\Big(\frac{\omega^2}{4c_0^2}\int_0^z \gamma_0(\boldsymbol{X}(z')) - \gamma_0(\boldsymbol{0})\mathrm{d}z'\Big) \simeq \exp\Big(-\frac{\gamma_0(\boldsymbol{0})\omega^2}{4c_0^2 l_{\rm cor}^2}\int_0^z |\boldsymbol{X}(z')|^2\mathrm{d}z'\Big),$$

for $\boldsymbol{X}(z') = \boldsymbol{y} - \boldsymbol{\xi}\frac{c_0 z'}{\omega}$. This is true when $|\boldsymbol{X}(z')|$ is small, and this is also true when it is not small in the sense that both members are of the order of $\exp(-\alpha z/l_{\rm sca})$ for some constant α and therefore they are both close to zero. As a result we find

$$\begin{aligned}\Gamma^{(2)}(\boldsymbol{x},\boldsymbol{y},z) &= \frac{r_{\rm ic}^2}{4\pi}\int_{\mathbb{R}^2}\exp\Big(i\boldsymbol{\xi}\cdot\boldsymbol{x} - \big(\frac{r_{\rm ic}^2}{4} + \frac{c_0^2 z^2}{4r_{\rm ic}^2\omega^2} + \frac{\gamma_0(\boldsymbol{0})z^3}{12l_{\rm cor}^2}\big)|\boldsymbol{\xi}|^2\\ &\quad + \big(\frac{c_0 z}{2\omega r_{\rm ic}^2} + \frac{\omega\gamma_0(\boldsymbol{0})z^2}{4c_0 l_{\rm cor}^2}\big)\boldsymbol{y}\cdot\boldsymbol{\xi} - \big(\frac{1}{4r_{\rm ic}^2} + \frac{\gamma_0(\boldsymbol{0})\omega^2 z}{4c_0^2 l_{\rm cor}^2}\big)|\boldsymbol{y}|^2\Big)\mathrm{d}\boldsymbol{\xi}.\end{aligned}$$

By taking $\boldsymbol{y} = \boldsymbol{0}$, we finally obtain

$$\begin{aligned}\mathbb{E}[|\hat{\phi}(\boldsymbol{x},z)|^2] &= \Gamma^{(2)}(\boldsymbol{x},\boldsymbol{0},z)\\ &= \frac{r_{\rm ic}^2}{4\pi}\int_{\mathbb{R}^2}\exp\Big(i\boldsymbol{\xi}\cdot\boldsymbol{x} - \big(\frac{r_{\rm ic}^2}{4} + \frac{c_0^2 z^2}{4r_{\rm ic}^2\omega^2} + \frac{\gamma_0(\boldsymbol{0})z^3}{12l_{\rm cor}^2}\big)|\boldsymbol{\xi}|^2\Big)\mathrm{d}\boldsymbol{\xi}\\ &= \frac{r_{\rm ic}^2}{R^2(\omega,z)}\exp\Big(-\frac{|\boldsymbol{x}|^2}{R^2(\omega,z)}\Big), \qquad (74)\end{aligned}$$

which is the desired result.

Appendix D. The case of identical media along the reference and signal paths. We briefly revisit the results of Section 7 to examine what would happen if the random media along the reference and signal paths were identical. In that case, the ghost imaging function would have the form (36) but the imaging kernel would be instead of (37):

$$\begin{aligned}H(\boldsymbol{x}_1,\boldsymbol{y}_3) &= \frac{c_0^4}{8\omega_0^4}\int_{\mathbb{R}^2}\mathrm{d}\boldsymbol{y}_1\int_{\mathbb{R}^2}\mathrm{d}\boldsymbol{y}_1'\int_{\mathbb{R}^2}\mathrm{d}\boldsymbol{y}_2\int_{\mathbb{R}^2}\mathrm{d}\boldsymbol{y}_2'\Gamma(\boldsymbol{y}_1,\boldsymbol{y}_2')\Gamma(\boldsymbol{y}_1',\boldsymbol{y}_2)\\ &\quad\times\mathbb{E}\big[\hat{g}\big(\omega_0,(\boldsymbol{x}_1,L),(\boldsymbol{y}_1,0)\big)\overline{\hat{g}\big(\omega_0,(\boldsymbol{x}_1,L),(\boldsymbol{y}_1',0)\big)}\\ &\quad\times\overline{\hat{g}\big(\omega_0,(\boldsymbol{y}_3,L),(\boldsymbol{y}_2',0)\big)}\hat{g}\big(\omega_0,(\boldsymbol{y}_3,L),(\boldsymbol{y}_2,0)\big)\big], \qquad (75)\end{aligned}$$

since now $\hat{g}_1 = \hat{g}_2 = \hat{g}$ where $\hat{g}$ is the solution of the Itô-Schrödinger equation (21). If Γ is given by (39) this can be simplified as

$$H(\boldsymbol{x}_1, \boldsymbol{y}_3) = \frac{c_0^4}{16\omega_0^4}\mathbb{E}\Big[\Big| \int_{\mathbb{R}^2} \exp\Big(-\frac{|\boldsymbol{y}|^2}{r_0^2}\Big)\hat{g}\big(\omega_0, (\boldsymbol{x}_1, L), (\boldsymbol{y}, 0)\big) \times \overline{\hat{g}\big(\omega_0, (\boldsymbol{y}_3, L), (\boldsymbol{y}, 0)\big)}\mathrm{d}\boldsymbol{y}\Big|^2\Big]. \tag{76}$$

The integral in $\boldsymbol{y}$ is the result of a time-reversal experiment using a point source at $(\boldsymbol{y}_3, L)$, a time-reversal mirror in the plane $z = 0$ with radius r_0, whose transverse spatial support is described by the function $\exp(-|\boldsymbol{y}|^2/r_0^2)$, and an observation point at $(\boldsymbol{x}_1, L)$. This time-reversal experiment is performed in a random medium and the waves travel through the same realization of the random medium during the forward propagation and during the backward propagation. We know that scattering is good in such a time-reversal configuration and that resolution can be enhanced compared to the homogeneous case [3, 7, 8]. In fact, using recent results on the fourth-order moments of the solution of the Itô-Schrödinger equation [13, Section 8, Proposition 1], we find here that, when $L \gg l_{\mathrm{sca}}$ and $l_{\mathrm{cor}} \ll r_0$,

$$H(\boldsymbol{x}_1, \boldsymbol{y}_3) = \mathcal{H}(\boldsymbol{x}_1 - \boldsymbol{y}_3), \qquad \mathcal{H}(\boldsymbol{x}) = \frac{I_0^2 r_0^4}{2^8\pi^2 L^4}\exp\Big(-\frac{|\boldsymbol{x}|^2}{4\rho_{\mathrm{gi3}}^2}\Big), \tag{77}$$

with the radius

$$\frac{1}{\rho_{\mathrm{gi3}}^2} = \frac{1}{\rho_{\mathrm{gi0}}^2} + \frac{16L}{l_{\mathrm{sca}} l_{\mathrm{cor}}^2}, \tag{78}$$

which shows that the radius of the convolution kernel is reduced by scattering and can even be smaller than the Rayleigh resolution formula.

REFERENCES

[1] D. G. Alfaro Vigo, J.-P. Fouque, J. Garnier and A. Nachbin, Robustness of time reversal for waves in time-dependent random media, *Stochastic Process. Appl.,* **113** (2004), 289–313.

[2] G. Bal and L. Ryzhik, Stability of time reversed waves in changing media, *Disc. Cont. Dyn. Syst. A,* **12** (2005), 793–815.

[3] P. Blomgren, G. Papanicolaou and H. Zhao, Super-resolution in time-reversal acoustics, *J. Acoust. Soc. Amer.,* **111** (2002), 230–248.

[4] M. Born and E. Wolf, *Principles of Optics*, Cambridge University Press, Cambridge, 1999.

[5] J. Cheng, Ghost imaging through turbulent atmosphere, *Opt. Express,* **17** (2009), 7916–7921.

[6] M. Fink, Time reversed acoustics, *Scientific American,* **281** (1999), 91–97.

[7] J.-P. Fouque, J. Garnier, G. Papanicolaou and K. Sølna, *Wave Propagation and Time Reversal in Randomly Layered Media*, Springer, New York, 2007.

[8] J. Garnier and G. Papanicolaou, Pulse propagation and time reversal in random waveguides, *SIAM J. Appl. Math.,* **67** (2007), 1718–1739.

[9] J. Garnier and G. Papanicolaou, Passive sensor imaging using cross correlations of noisy signals in a scattering medium, *SIAM J. Imaging Sciences*, **2** (2009), 396–437.

[10] J. Garnier and G. Papanicolaou, Resolution analysis for imaging with noise, *Inverse Problems*, **26** (2010), 074001, 22pp.

[11] J. Garnier and G. Papanicolaou, Fluctuation theory of ambient noise imaging, *CRAS Geoscience*, **343** (2011), 502–511.

[12] J. Garnier and K. Sølna, Coupled paraxial wave equations in random media in the white-noise regime, *Ann. Appl. Probab.*, **19** (2009), 318–346.

[13] J. Garnier and K. Sølna, Fourth-moment analysis for wave propagation in the white-noise paraxial regime, *Arch. Rational Mech. Anal.,* **220** (2016), 37–81.

[14] N. D. Hardy and J. H. Shapiro, Reflective Ghost Imaging through turbulence, *Phys. Rev. A*, **84** (2011), 063824.

[15] P. Hariharan, *Optical Holography*, Cambridge University Press, Cambridge, 1996.

[16] A. Ishimaru, *Wave Propagation and Scattering in Random Media*, IEEE Press, Piscataway, 1997.
[17] O. Katz, Y. Bromberg and Y. Silberberg, Compressive ghost imaging, *Appl. Phys. Lett.*, **95** (2009), 131110.
[18] C. Li, T. Wang, J. Pu, W. Zhu and R. Rao, Ghost imaging with partially coherent light radiation through turbulent atmosphere, *Appl. Phys. B*, **99** (2010), 599–604.
[19] L. Mandel and E. Wolf, *Optical Coherence and Quantum Optics*, Cambridge University Press, Cambridge, 1995.
[20] J. H. Shapiro, Computational ghost imaging, *Phys. Rev. A*, **78** (2008), 061802(R).
[21] J. H. Shapiro and R. W. Boyd, The physics of ghost imaging, *Quantum Inf. Process.*, **11** (2012), 949–993.
[22] F. D. Tappert, The parabolic approximation method, in *Wave Propagation and Underwater Acoustics*, Springer Lecture Notes in Physics, **70** (1977), 224–287.
[23] V. I. Tatarski, *Wave Propagation in a Turbulent Medium*, Dover, New York, 1961.
[24] B. J. Uscinski, *The Elements of Wave Propagation in Random Media*, McGraw Hill, New York, 1977.
[25] A. Valencia, G. Scarcelli, M. D'Angelo and Y. Shih, Two-photon imaging with thermal light, *Phys. Rev. Lett.*, **94** (2005), 063601.
[26] P. Zhang, W. Gong, X. Shen and S. Han, Correlated imaging through atmospheric turbulence, *Phys. Rev. A,* **82** (2010), 033817.

Received for publication October 2014.

E-mail address: garnier@math.univ-paris-diderot.fr